Myeloid HDAC7 drives liver inflammation and systemic glucose dysregulation during diet-induced obesity

Yizhuo Wang[1,2,a], Divya Ramnath[1,2], Kaustav Das Gupta[1,2,b], P. Prakrithi[1,3], Kavita Bisht[4], Gregory C. Miller[5,6], Zherui Xiong[1,3], Yujun Wan[7,c], Ellen N. Tejo[4], James E.B. Curson[1,2], Rishika Abrol[1,2], Sahar Keshvari[4], Kimberley S. Gunther[1,2], Jordan D. Atkinson[1,2], Zhixuan Loh[1], Jessica A. Engel[3], Christian R. Engwerda[3], Sabrina Sofia Burgener[1,2], Kate Schroder[1,2], David P. Fairlie[1,2], Andrew D. Clouston[5,6], Elizabeth E. Powell[3,6,8], Katharine M. Irvine[4], Mitchell A. Sullivan[4,9,10], Jean-Pierre Lévesque[4], Quan Nguyen[1,3], Matthew J. Sweet[1,2,#] and Denuja Karunakaran[1,11,12,d,#]

Affiliations

[1]Institute for Molecular Bioscience, The University of Queensland, Brisbane, Queensland, Australia.

[2]Australian Infectious Diseases Research Centre, The University of Queensland, Brisbane, Queensland, Australia.

[3]QIMR Berghofer Medical Research Institute, Brisbane, Queensland, Australia.

[4]Mater Research Institute-UQ, Translational Research Institute, Brisbane, Queensland, Australia.

[5]Envoi Specialist Pathologists, Brisbane, Queensland, Australia.

[6]Faculty of Health, Medicine and Behavioural Sciences, The University of Queensland, Brisbane, Queensland, Australia.

[7]Centre for Nutrition and Food Sciences, Queensland Alliance for Agriculture and Food Innovation, The University of Queensland, Brisbane, Queensland, Australia.

[8]Department of Gastroenterology and Hepatology, Princess Alexandra Hospital, Brisbane, Queensland, Australia.

[9]Centre for Bioinnovation and School of Health, University of the Sunshine Coast, Sippy Downs, Queensland, Australia.

[10]Sunshine Coast Health Institute, Birtinya, Queensland, Australia.

[11]Department of Physiology, Monash Biomedicine Discovery Institute, Monash University, Melbourne, Australia.

[12]Victorian Heart Institute, Victorian Heart Hospital, Melbourne, Australia.

[a]Present address: QIMR Berghofer Medical Research Institute, Brisbane, Queensland, Australia.

[b]Present address: Division of Infectious Disease, The Lundquist Institute for Biomedical Innovation at Harbor-University of California, Los Angeles Medical Center, Torrance, California, USA.

[c]Present address: Department of Biochemistry, School of Biological Sciences, University of Cambridge, Cambridge CB2 1QW, United Kingdom.

[d]Present address: Department of Physiology, Monash Biomedicine Discovery Institute, Monash University, Melbourne, Australia.

[#]Address correspondence to Matthew J Sweet: m.sweet@imb.uq.edu.au or Denuja Karunakaran: denuja.karunakaran@monash.edu

Abstract

Objectives: Histone deacetylase 7 (HDAC7), a classical HDAC family member, promotes LPS-inducible glycolysis and inflammatory mediator production in macrophages, innate immune cells that contribute to pathology in metabolic diseases. Here, we investigated myeloid HDAC7 functions in obesity-driven metabolic disease.

Methods: We used gain- and loss-of-function genetic approaches in mice to investigate myeloid HDAC7 functions in hepatic inflammation and metabolic disease, as well as associations with hepatic gene signatures characteristic of advanced chronic liver disease (CLD).

Results: Transgenic expression of *Hdac7* in myeloid cells increased liver inflammation and liver mRNA levels of *Ccl2* and *Il1b*, key inflammatory mediators linked to CLD. Liver glycogen levels were also decreased, another feature of CLD. Transgenic expression of *Hdac7* in myeloid cells mimicked the hepatic inflammatory phenotype that was observed in mice fed a high fat, high cholesterol, and high sucrose (HFHCHS) diet, an obesity model that mimics some features of metabolic dysfunction-associated steatotic liver disease. In myeloid *Hdac7* transgenic mice fed a HFHCHS diet, relative weight gain was increased, fasted glucose levels were elevated and glucose tolerance was dysregulated by comparison to control mice. Conversely, fasted blood glucose levels were reduced and glucose tolerance was improved in myeloid *Hdac7*-deleted mice on a HFHCHS diet. *HDAC7* mRNA levels were also elevated in the livers of people with advanced CLD and spatial transcriptomics revealed that myeloid HDAC7 directs hepatic gene signatures characteristic of advanced CLD.

Conclusions: Myeloid HDAC7 contributes to hepatic inflammation and systemic glucose dysregulation in a mouse model of obesity and liver inflammation.

Keywords: glucose metabolism; histone deacetylase 7; inflammation; macrophages; metabolic dysfunction-associated steatotic liver disease; obesity

72 **Introduction**

73 Metabolic dysfunction-associated steatotic liver disease (MASLD) is a common cause of
74 chronic liver disease (CLD) that is associated with substantial morbidity and mortality[1].
75 MASLD progressing to metabolic dysfunction-associated steatohepatitis (MASH) is the major
76 cause of cirrhosis, especially in developed countries[2]. MASLD represents a spectrum of
77 conditions, ranging from fatty liver (steatosis) without significant inflammation to MASH,
78 where liver injury, inflammation, and/or fibrosis accompany steatosis[3]. The thyroid hormone
79 receptor-β agonist Resmetirom[4] and the glucagon-like peptide-1 (GLP-1) receptor agonist
80 semaglutide[5] are approved in the USA as therapies for patients with moderate to advanced liver
81 fibrosis. Other therapies are currently under clinical evaluation[6], including tirzepatide, a dual
82 agonist for GLP-1 and glucose-dependent insulinotropic polypeptide receptors[7]. However,
83 these therapies are likely to be effective in only a sub-set of MASH patients. The development
84 of more effective treatments requires a better understanding of the complex underlying
85 mechanisms that drive MASH and the employment of approaches that target multiple
86 inflammatory and fibrotic pathways.

87

88 Macrophages are key innate immune cells that sense and respond to endogenous and exogenous
89 danger signals, enabling them to detect perturbations in homeostasis[8]. These cells are extremely
90 heterogeneous, exhibiting diverse phenotypes depending on the specific environmental
91 conditions encountered[9]. Liver macrophages, comprising both tissue-resident Kupffer cells and
92 monocyte-derived macrophages, play important roles in liver homeostasis and in responding
93 to environmental signals. Kupffer cells clear endotoxin and phagocytose bacterial pathogens,
94 dying cells and other debris in the hepatic parenchyma[10, 11], and also release inflammatory
95 cytokines upon activation via the pattern recognition receptors, such as toll-like receptor (TLR)
96 4[12]. Recruited monocytes can also differentiate into macrophages in the liver, either promoting
97 wound healing and tissue repair when the injury-inducing agents have been removed[13, 14] or
98 perpetuating inflammation and pathology during active disease[15, 16]. A failure to resolve
99 macrophage activation leads to dysregulated production of inflammatory mediators that
100 contribute to pathological conditions, including liver fibrosis[10]. For example, elevated TNF
101 levels in inflamed livers contribute to fibrogenesis[17], the chemokine CCL2 promotes lipid
102 accumulation in hepatocytes leading to obesity-induced liver steatosis[18] and MASH
103 progression[19], and inflammasome-mediated IL-1β production is associated with collagen
104 deposition in MASH patients[20]. Targeting of such inflammatory mediators can attenuate

105 progression of liver disease in mouse models. For example, inhibition of IL-1 receptor
106 signalling[21] or deletion of *Il1b* that encodes IL-1β[22] in mouse models limited MASH
107 progression.
108
109 To fuel proinflammatory responses, aerobic glycolysis is rapidly increased in TLR-activated
110 macrophages[23, 24]. This is linked with TCA cycle reprogramming, ultimately resulting in the
111 generation of acetyl-CoA that enables histone modifications for inducible expression of
112 inflammatory genes[25, 26]. Signalling molecules that connect glycolysis and inflammation such
113 as the glycolytic enzyme pyruvate kinase isoform 2 (PKM2) have been implicated in the
114 pathogenesis of MASH. For example, elevated levels of PKM2 in both serum and liver were
115 associated with MASLD severity[27]. PKM2 exists in two forms, a tetramer that is associated
116 with its glycolytic function and a dimeric form that drives inflammatory responses. Tetrameric
117 PKM2 polarises macrophages towards a regulatory or anti-inflammatory phenotype,
118 ameliorating liver inflammation and steatosis[28]. In contrast, nuclear accumulation of dimeric
119 PKM2 in macrophages was reported to promote macrophage polarisation towards a pro-
120 inflammatory phenotype, leading to MASH pathogenesis[29]. Significantly, a group of proteins
121 called the class IIa histone deacetylases (HDACs) promote dimerization and activation of the
122 pro-inflammatory form of PKM2 in macrophages[30].
123
124 HDACs remove an acetyl moiety from the ε-amino group of lysine residues of histones, with
125 this generally associated with repression of gene transcription[31]. However, thousands of non-
126 histone proteins are also regulated by lysine acetylation[32, 33], so HDACs control many cellular
127 processes beyond gene expression. Class IIa HDACs are a subfamily of the classical HDACs
128 that share a conserved C-terminal deacetylase domain and a less conserved N-terminus that
129 interacts with a broad range of cellular proteins[34], allowing this family to regulate various
130 biological processes in physiological and pathological conditions (reviewed in[35, 36]). One class
131 IIa HDAC with a particularly important function in metabolic and inflammatory processes in
132 macrophages is HDAC7 (reviewed in[37, 38]). In human and murine macrophages, HDAC7
133 orchestrates LPS-induced glycolysis and the production of key inflammatory mediators IL-1β
134 and CCL2[30], two inflammatory mediators associated with MASLD/MASH. Interestingly,
135 HDAC7 primarily functions in macrophages responding to submaximal concentration of
136 LPS[39], suggesting that this class IIa HDAC may be particularly important in driving chronic
137 low-grade inflammation. In contrast, HDAC7 engages the pentose phosphate pathway in
138 macrophages responding to bacterial challenge, with this enabling pathogen destruction and

139 attenuation of inflammation[40]. This highlights a role for HDAC7 in context-dependent danger
140 recognition during inflammation, meaning that predicting its function in different disease
141 settings such as MASLD/MASH is not straightforward. In this study, using myeloid *Hdac7*
142 gain- and loss-of-function mice, we reveal a role for myeloid HDAC7 in liver inflammation
143 and glucose dysregulation in an obesity model that shares some features with MASLD.

144 ## Results

145 **Myeloid *Hdac7* overexpression promotes liver inflammation in mice**

146 We previously showed that HDAC7 drives production of the pro-inflammatory mediators
147 CCL2 and IL-1β in TLR4-activated macrophages[30, 39] and that acute LPS-induced systemic
148 inflammation was amplified in MacHDAC7 mice that selectively over-express HDAC7 in
149 myeloid cells[30]. However, whether myeloid HDAC7 drives inflammatory responses and/or
150 pathological changes in the liver has not been examined. To determine if myeloid HDAC7
151 might contribute to chronic and low-grade liver inflammation, we utilised MacHDAC7
152 transgenic mice[30] that overexpress an alternatively spliced, inflammatory form of mouse
153 HDAC7 lacking the first 22 amino acids, HDAC7-u[41], in myeloid cells. In MacHDAC7 mice,
154 *Csf1r* promoter elements direct myeloid-specific expression of the transcriptional activator
155 GAL4-VP16, which in turn drives both HDAC7-u and cyan fluorescent protein (CFP)
156 expression in myeloid cells. Littermate MacBlue mice that express GAL4-VP16-dependent
157 CFP expression were used as controls in these studies[42]. We first evaluated the expression of
158 inflammatory mediators and markers of liver fibrosis in naïve MacBlue and MacHDAC7 mice.
159 As expected, mRNA levels of *Hdac7* were significantly elevated in the livers of MacHDAC7
160 mice compared to those of MacBlue control mice (**Figure 1A**). Thus, the effect of myeloid-
161 specific *Hdac7* overexpression could be detected at the whole-organ level, even in the context
162 of endogenous *Hdac7* expression in hepatocytes and other non-myeloid cells. Consistent with
163 the elevated systemic levels of inflammatory mediators observed upon LPS challenge in
164 MacHDAC7 mice[30], mRNA levels of the inflammatory genes *Ccl2* and *Il1b* were increased in
165 livers of these mice in a basal state (**Figure 1B-C**). Of the fibrotic genes that were examined,
166 only *Mmp9* was increased (**Figure 1D**), with no difference being observed between the two
167 genotypes in mRNA levels of other inflammatory or fibrotic genes such as *Crp*, *Fstl1*, *Col1a1*
168 and *Act2* (**Figure S1**). Thus, myeloid *Hdac7* overexpression increases levels of specific
169 inflammatory mediators in the liver, suggesting that it may prime liver inflammation and/or
170 accelerate liver disease under certain conditions.

171

172 **Myeloid *Hdac7* overexpression increases weight gain in mice fed a HFHCHS diet**

173 To mimic the metabolic and histological changes of MASLD, we placed littermate
174 MacHDAC7 and MacBlue control mice at 6-10 weeks of age on a HFHCHS diet (20% kcal
175 fat, 20 g/kg cholesterol, 222 g/kg fructose and 107 g/kg sucrose) for 24 wk, with weekly body
176 weight gain and metabolic parameters measured. As basal inflammatory mediators were

elevated in livers of MacHDAC7 mice (**Figure 1**), cohorts of MacHDAC7 and MacBlue control mice fed on a chow diet were also included. Body weights of mice of each genotype were similar at the onset of the experiment (**Figure 2A**). As expected, the HFHCHS diet increased body weight for both genotypes by comparison to their respective chow diet groups. However, weight gain of MacHDAC7 mice fed on either a chow or HFHCHS diet was significantly reduced by comparison to the control MacBlue mice (**Figure 2A**). When correcting for this difference by normalizing the HFHCHS-dependent gain to the chow trajectory for each genotype, MacHDAC7 mice displayed a significantly greater relative weight gain on the HFHCHS diet than MacBlue over the 24 weeks of the experiment (**Figure 2B**). To study whole-body metabolism, fat and lean mass was also measured. Interestingly, *Hdac7* overexpression in myeloid cells reduced both the fat and lean mass in mice fed a chow diet (**Figure 2C**, left), consistent with the smaller average body weight of MacHDAC7 mice. This difference was not apparent in mice fed a HCHFHS diet (**Figure 2C**, right), suggesting that this diet increased both fat and lean body compositions in MacHDAC7 mice to a greater extent than MacBlue control mice.

The HFHCHS diet also significantly increased the weights of liver and epididymal white adipose tissue (WAT) in both MacBlue and MacHDAC7 mice (**Figure 2D-E**), but this diet led to increased kidney weights only in MacHDAC7 mice (**Figure 2F**). This may reflect diet-induced renal damage. When normalising to the average tissue weight of chow-fed controls, the HFHSHC diet resulted in a modest, non-significant increase in epididymal fat weight for MacHDAC7 versus MacBlue mice (MacBlue 176.7% ± 46.3% vs. MacHDAC7 281.5% ± 56.3%, $p = 0.07$, Student's t-test). In contrast, kidney weight was markedly elevated (MacBlue 9.87% ± 6.1% vs. MacHDAC7 27.0% ± 3.9%, $p = 0.01$, Student's t-test). Interestingly, splenomegaly was observed in the MacHDAC7 mice when fed a chow diet (**Figure 2G**). This is suggestive of perturbed haematopoiesis in these mice, which would be consistent with *Hdac7*-induced liver inflammation in the basal state (**Figure 1**). We therefore next investigated the impact of HDAC7 overexpression on immune cell profiles. MacHDAC7 mice on the chow diet exhibited significant neutrophilia in peripheral blood, similar to levels observed for both MacBlue and MacHDAC7 mice on the HFHCHS diet (**Table 1**). This is consistent with a primed immune state that may drive low-grade myeloid inflammation associated with increased adiposity. Collectively, these data implicate myeloid *Hdac7* in both limiting weight gain of mice on a chow diet, as well enhancing relative weight gain of mice

210 under HFHCHS. Both of these phenotypes could relate to HDAC7-driven inflammation and
211 immune cell expansion.
212
213 **Myeloid *Hdac7* overexpression drives neutrophilia and perturbs haematopoiesis**
214 The immune profiling above was performed on mice aged 30-34 weeks, so it was conceivable
215 that the observed neutrophilia was an age-assocated phenomenon. To investigate this, we
216 assessed immune profiles of peripheral blood from 6-8 week old mice. Here we found that
217 MacHDAC7 mice exhibited pronounced leukocytosis ($p < 0.01$) and neutrophilia ($p < 0.05$)
218 compared with MacBlue controls, whereas there were no significant differences in monocytes,
219 eosinophils, basophils and lymphocytes (**Table 2**). Young adult MacHDAC7 mice (6-10 week
220 old) also showed marked splenomegaly versus MacBlue control mice (~3-fold increase in
221 spleen weight; $p < 0.0001$), with this accompanied by a substantial expansion of total
222 splenocytes and splenic immune subsets, including $B220^+$ B cells, $CD3^+$ T cells, and $CD11b^+$
223 myeloid cells ($p < 0.0001$) (**Table 3**). Thus, MacHDAC7 mice exhibit marked splenomegaly
224 with broad immune-cell expansion and circulating leukocytosis dominated by neutrophils,
225 indicative of a systemic immune-primed state.
226
227 **Myeloid *Hdac7* promotes hepatic inflammation but not fibrosis in mice**
228 Given that HDAC7 drives inflammatory responses in primary macrophages[30, 39], we postulated
229 that myeloid *Hdac7* overexpression alone may amplify diet-induced liver inflammation. As we
230 previously observed (**Figure 1**), mRNA levels of *Ccl2* and *Il1b* were elevated in MacHDAC7
231 mice fed a chow diet compared to MacBlue control mice (**Figure 3A-B**). Interestingly, this
232 difference was not apparent in mice fed a HFHCHS diet, suggesting that myeloid *Hdac7* alone
233 primed liver inflammation. CCL2 and the accompanying infiltration of inflammatory
234 monocytes contributes to MASH in animal models[43, 44]. We therefore assessed circulating
235 CCL2 levels. MacHDAC7 mice fed a chow diet had significantly higher levels of serum CCL2
236 than the MacBlue control mice (**Figure 3C**). This effect was also apparent in mice fed the
237 HFHCHS diet, although it was less pronounced because the HFHCHS diet increased CCL2
238 production in MacBlue mice. Consistent with its effects on hepatic *Ccl2* mRNA expression
239 (**Figure 3A**) and circulating CCL2 (**Figure 3C**), hepatic mRNA levels of *Adgre1* that encodes
240 the tissue macrophage marker F4/80 and Kupffer cell-restricted *Clec4f* were both elevated in
241 MacHDAC7 mice versus MacBlue mice fed a chow diet (**Figure 3D-E**). Serum IL-1β levels
242 were below the limits of detection in these samples (data not shown), but overall, the results
243 suggest that myeloid *Hdac7* overexpression alone broadly phenocopies hepatic inflammation

triggered by the HFHCHS diet. This was supported by blinded histological analyses, where liver inflammation was similar between MacHDAC7 mice on a chow diet and MacBlue control mice on a HFHCHS diet (**Figure 3F-G**).

Having established a role for myeloid HDAC7 in driving liver inflammation, we next assessed its role in liver steatosis and fibrosis. Here we found that the HFHCHS diet induced lipid accumulation and liver steatosis in both MacBlue and MacHDAC7 mice, but this effect was not amplified by *Hdac7* overexpression (**Figure 3H-J**). This suggests that myeloid *Hdac7* overexpression does not have obvious effects on lipid metabolism in the liver. Although histological examination revealed that myeloid *Hdac7* overexpression did not exacerbate HFHCHS-induced liver inflammation (**Figure 3F-G**), we did observe a modest and non-significant increase in NAFLD activity score in MacHDAC7 mice fed a chow diet by comparison to versus MacBlue control mice (**Figure 3K**). However, the HFHCHS diet failed to induce a constant and robust MASH-like phenotype in either group, as shown by the mild and highly variable levels of fibrosis (**Table S1**), thus it remains unclear whether myeloid *Hdac7* promotes diet-induced MASH. Taken together, these observations suggest that myeloid *Hdac7* overexpression promotes hepatic and systemic inflammation, but this alone is not sufficient to drive liver fibrosis.

Glucose metabolism is dysregulated in MacHDAC7 mice fed a HFHCHS diet

Insulin resistance is a common metabolic syndrome of MASLD[45]. Thus, we measured fasted blood glucose levels to assess whether myeloid *Hdac7* overexpression regulates hepatic glucose metabolism. When placed on a chow diet, MacHDAC7 mice consistently had lower fasted blood glucose levels than the control MacBlue mice, with these effects being significant at wk 4 and 16 (**Figure 4A**). To assess glucose clearance, we performed intraperitoneal glucose tolerance tests (GTTs) at wk 12, finding that the MacHDAC7 mice cleared injected glucose more rapidly than the MacBlue control, albeit the difference was not statistically significant (**Figure 4B**). However, these phenotypes were reversed when mice were fed a HFHCHS diet, with higher blood glucose levels and slower glucose clearance observed in MacHDAC7 mice (**Figure 4C-D**). This suggests that myeloid HDAC7 has context-dependent roles in regulating glucose metabolism.

In a fasting state, glucose is mainly produced in the liver via glycogenolysis and gluconeogenesis, with the former converting glycogen into glucose[46]. We therefore considered

278 that hyperglycaemia in the MacHDAC7 mice fed a HFHCHS diet could be due to a change in
279 hepatic glycogen metabolism. Interestingly, MacHDAC7 mice had lower liver glycogen levels
280 than MacBlue control mice when fed the chow diet, with a similar non-significant trend being
281 apparent for mice fed the HFHCHS diet (**Figure 4E**). It is therefore likely that myeloid HDAC7
282 plays a role in glycogen metabolism in both lean and obese mice. Hyperglycaemia inhibits
283 glycogenolysis in healthy individuals, with this inhibition being impaired in type 2 diabetes
284 mellitus[47]. Since MacHDAC7 mice fed a HFHCHS diet had lower hepatic glycogen levels
285 (**Figure 4E**) and increased fasting glucose levels (**Figure 4C**) than MacBlue mice, we propose
286 that regulatory control of hepatic glycogen breakdown may be impaired in MacHDAC7 mice,
287 leading to enhanced glycogenolysis. We conclude that myeloid HDAC7 overexpression
288 exacerbates HFHCHS diet-induced dysregulation of glucose and glycogen metabolism.
289
290 Inflammatory mediators such as CCL2 promote macrophage infiltration, hepatic inflammation,
291 and insulin resistance during diet-induced obesity[48, 49]. Considering the role of HDAC7 in
292 macrophage inflammation and that myeloid *Hdac7* expression triggered higher levels of
293 circulating CCL2 (**Figure 3C**), we next wondered whether myeloid *Hdac7* alters insulin
294 secretion during obesity. Indeed, insulin levels were reduced in MacHDAC7 mice versus
295 MacBlue control mice fed a chow diet (**Figure 4F**, centre). This suggests that lean MacHDAC7
296 mice (**Figure 2C**) control insulin levels to respond to their lower blood glucose levels (**Figure**
297 **4A**). Interestingly, when fed a HFHCHS diet, both MacBlue and MacHDAC7 mice had
298 similarly elevated insulin levels (**Figure 4F**, right), suggesting a feedback mechanism of
299 increased insulin production to suppress elevated blood glucose levels. However, these
300 increased insulin levels failed to control glucose production in MacHDAC7 mice (**Figure 4C**).
301 We conclude that elevated HDAC7 expression in myeloid cells drives metabolic dysregulation,
302 a feature of type 2 diabetes mellitus[50].
303
304 **Myeloid *Hdac7* deletion does not alter weight gain but attenuates HFHCHS diet-induced**
305 **glucose dysregulation**
306 Given that myeloid *Hdac7* overexpression triggered neutrophilia and hepatic inflammation, as
307 well as dysregulated glucose homeostasis in diet-induced obesity, we hypothesised that
308 genetically targeting *Hdac7* in myeloid cells would ameliorate HFHCHS-induced phenotypes.
309 To test this, we used myeloid-restricted *Hdac7*$^{-/-}$ mice (*Hdac7*$^{fl/fl}$ *LysM*^{Cre}) and littermate
310 *Hdac7*$^{+/+}$ control mice (*Hdac7*$^{fl/fl}$), placing the mice on a HFHCHS diet for a period of 36 wk
311 with the goal of inducing more severe MASH phenotypes. In contrast to the increased relative

312 weight gain of myeloid HDAC7 gain-of-function mice on a HFHCHS versus chow diet (**Figure**
313 **2B**), *Hdac7* deletion from myeloid cells did not affect weight gain in mice fed a HFHCHS diet
314 (**Figure S2A**). Similarly, fat and lean mass (**Figure S2B**) and organ weights (**Figure S2C**) were
315 unaffected, although there was a modest trend towards reduced liver mass. These data indicate
316 that myeloid *Hdac7* deficiency does not prevent the development of obesity.
317
318 Next, we examined glucose metabolism to determine whether myeloid *Hdac7* deletion
319 improves the dysregulated phenotypes induced by the HFHCHS diet. *Hdac7*$^{-/-}$ mice had similar
320 blood glucose levels to the control mice at the beginning of the study (**Figure 5A**, 0 wk).
321 However, starting from wk 8 of HFHCHS feeding, myeloid-restricted *Hdac7*$^{-/-}$ mice had
322 consistently lower fasted blood glucose levels than *Hdac7*$^{+/+}$ mice, with the effects being
323 significant at wk 8, 14 and 16 (**Figure 5A**). This suggests that deletion of *Hdac7* from myeloid
324 cells improves blood glucose regulation. This effect was also reflected in improved glucose
325 tolerance in *Hdac7*$^{-/-}$ mice (**Figure 5B-C**). *Hdac7*$^{-/-}$ mice also presented with slightly improved
326 insulin sensitivity than control mice, although these effects were not significant (**Figure 5D-**
327 **E**). Hence, myeloid deletion of *Hdac7* reduces fasting glucose and improves glucose
328 intolerance in the HFHCHS obesity model.
329
330 **Myeloid *Hdac7* deletion did not ameliorate diet-induced hepatic pathology and**
331 **inflammation**
332 Next, we assessed whether the effects of *Hdac7* deletion on glucose metabolism may relate to
333 inflammation. At the cellular level, levels of HDAC7 protein were greatly reduced in bone
334 marrow derived macrophages (BMMs) from *Hdac7*$^{-/-}$ mice fed on both HFHCHS and chow
335 diets, as expected (**Figure S3A**). Consistent with previous findings[30], LPS-inducible CCL2 and
336 inflammasome-triggered IL-1β levels were reduced in BMMs from the naïve *Hdac7*$^{-/-}$ mice on
337 a chow diet (**Figure S3B**, right side of graphs). However, in *Hdac7*$^{-/-}$ BMMs generated from
338 mice fed the HFHCHS diet, only IL-1β levels were significantly reduced, with CCL2 levels
339 being only marginally affected (**Figure S3B**, left side of graphs). These data indicate that the
340 capacity of HDAC7 to drive the production of these inflammatory mediators in macrophages
341 may be attenuated under the conditions of obesity. Consistent with this, hepatic *Ccl2* mRNA
342 levels were only slightly reduced in myeloid *Hdac7*$^{-/-}$ mice (**Figure S3C**). Liver *Il1b* mRNA
343 levels (**Figure S3D**) and circulating CCL2 levels (**Figure S3E**) were also unaffected.
344 Histological assessment of livers from these mice revealed that the HFHCHS diet induced only
345 varying levels of early to moderate stages of liver fibrosis in mice from either genotype (**Figure**

346 **S4A**). Of note, the *Hdac7*$^{-/-}$ mice trended towards a very modest reduction in liver inflammation,
347 lipid accumulation, steatosis and fibrosis compared to the *Hdac7*$^{+/+}$ control mice (**Figure S4B-**
348 **F**). This suggests that myeloid *Hdac7* deletion may very modestly reduce obesity-induced
349 pathological processes in the liver. We conclude that myeloid HDAC7 drives glucose
350 dysregulation but only marginally contributes to hepatic inflammation and fibrosis in the
351 HFHCHS diet model.
352
353 **Myeloid *HDAC7* expression is associated with gene expression signatures linked to**
354 **advanced CLD**
355 Our data support a role for HDAC7 in mediating glucose dysregulation in both gain- and -loss
356 of function mouse models, as well as liver inflammation in a gain-of-function mouse model.
357 We therefore considered that elevated HDAC7 expression in CLD may contribute to metabolic
358 dysregulation and/or disease progression. We thus assessed *HDAC7* mRNA levels in liver
359 biopsies of people with early or advanced CLD[51]. Here we found that *HDAC7* mRNA levels
360 were elevated in livers from people with advanced CLD by comparison to those with early
361 disease (**Figure 6A**), suggestive of a link between HDAC7 and human CLD severity. To further
362 investigate this link in myeloid cells, we performed spatial transcriptomic analysis on livers
363 from MacBlue and MacHDAC7 mice fed a chow diet to identify myeloid HDAC7-associated
364 transcriptional changes relevant to CLD. We first identified cells co-expressing *eCFP* and
365 *Hdac7* mRNAs in livers, then performed differential gene expression analysis on
366 *eCFP*$^{+}$/*Hdac7*$^{+}$ cells from MacBlue versus MacHDAC7 mice. A heatmap of the 53
367 differentially expressed genes is shown in **Figure 6B**. This analysis confirmed elevated *Il1b*,
368 *Ccl2* and *Mmp9* mRNA levels in hepatic myeloid cells from MacHDAC7 mice (**Figure 6B**),
369 consistent with our previous findings in whole liver tissue (**Figure 1B-D**). When compared
370 with our previously published dataset of genes associated with early and advanced human
371 CLD[51], we found that eight genes associated with advanced CLD in human were also
372 differentially expressed in *eCFP*$^{+}$ cells in livers of MacHDAC7 mice. These include *Vcan*,
373 *Thbs1*, *Mmp9* and *Rab8b* (**Figure 6B**), several of which have been implicated in CLD
374 progression and/or pathology[52-54]. Spatial co-expression analysis revealed that these genes
375 were co-expressed with HDAC7, with limited expression in other hepatic cells (**Figure 6C-F**).
376 This suggests that myeloid HDAC7 expression is sufficient to direct gene expression programs
377 associated with advanced CLD. In summary, data presented in this study implicate myeloid
378 HDAC7 in driving hepatic inflammation and expression of genes linked to advanced CLD, as
379 well as systemic glucose dysregulation in a mouse obesity model.

380 **Discussion**

381 In this study, we investigated potential roles of myeloid HDAC7 in metabolic diseases,
382 examining obesity, glucose dysregulation, hepatic inflammation and fibrosis. Although levels
383 of steatosis and fibrosis were variable in our studies (**Figure 3H-K, S4C-F, Table S1**),
384 HFHCHS fed mice did develop diet-induced obesity (**Figure 2A**) and liver inflammation
385 (**Figure 3F-G**). We therefore focused our studies on indicators of metabolism and
386 inflammation. We found the overexpression of myeloid *Hdac7* promoted hepatic inflammation
387 (**Figure 3**) and expansion of leukocytes, particularly neutrophils (**Tables 1-2**), in a basal state,
388 sharing some overlap with phenotypes observed in control MacBlue mice under HFHCHS. We
389 also observed that weight gain of MacHDAC7 mice fed either a chow or HFHCHS diet was
390 reduced by comparison to MacBlue mice (**Figure 2A**), which may relate to the energetic burden
391 required for immune cell expansion. These findings complicate interpretation of the effects of
392 HDAC7 on HFHCHS diet-induced weight gain, though we note that the relative increase in
393 body weight (HFHCHS versus chow diet) was significantly increased in MacHDAC7 versus
394 MacBlue mice (**Figure 2B**). Of note, in the HFHCHS diet model, glucose dysregulation was
395 exacerbated in myeloid HDAC7 gain-of-function mice and improved in myeloid HDAC7 loss-
396 of-function mice. This key finding thus extends the functions of HDAC7 in macrophages
397 beyond cellular metabolism[30, 39, 40] to whole body glucose metabolism.

398

399 MacHDAC7 mice on a HFHCHS diet had increased hyperglycaemia at multiple time points
400 (**Figure 4C**), as well as impaired glucose tolerance (**Figure 4D**), by comparison to MacBlue
401 control mice. Conversely, hyperglycaemia (**Figure 5A**) and glucose clearance (**Figure 5B**)
402 were improved in myeloid *Hdac7*$^{-/-}$ mice on a HFHCHS diet. Collectively, these data implicate
403 myeloid HDAC7 as a contributor to glucose dysregulation during obesity. Interestingly,
404 MacHDAC7 mice on a chow diet had reduced levels of fasted blood glucose (**Figure 4A**) and
405 liver glycogen (**Figure 4E**), suggesting that glycogen metabolism is disrupted in these mice.
406 Under fasting conditions, glycogenolysis is initiated by glucagon and epinephrine-dependent
407 cascades[55]. Glycogen phosphorylase is a key enzyme controlling glycogenolysis, converting
408 glycogen to glucose-1-phosphate, which is subsequently converted to glucose-6-phosphate that
409 feeds glycolysis[56]. A previous study found that glycogen phosphorylase activity is controlled
410 by post-translational modifications. Specifically, acetylation at K470 inhibits its enzymatic
411 activity, with this inactivation mechanism being enhanced by insulin[57]. MacHDAC7 mice on
412 the chow diet had significantly lower blood insulin levels than control MacBlue mice, with this

413 difference being absent in mice fed the HFHCHS diet (**Figure 4F**). Thus, we propose that
414 myeloid HDAC7 may somehow limit insulin secretion in MacHDAC7 mice to indirectly
415 enhance glycogenolysis in hepatic cells. This hypothesis will need to be tested in future studies
416 to characterise hepatic glycogen content and flux, as well as molecular mechanisms involved.
417 Alternatively, it is also possible that HDAC7 promotes glycogen breakdown in macrophages,
418 which could contribute to glucose dysregulation in the setting of obesity. Activated
419 macrophages have been shown to store glycogen and metabolise it to drive inflammatory
420 responses via multiple mechanisms[58]. Thus, HDAC7-mediated glycogenolysis in macrophages
421 could contribute to both dysregulated inflammation and glucose metabolism during obesity.
422 We previously showed that HDAC7 increases the enzymatic activity of the glycolytic enzyme
423 PKM2 by interacting with it and promoting its deacetylation[30] and it is possible that HDAC7
424 similarly activates enzymes in the glycogenolysis pathway in macrophages.
425
426 In the fasting state, another source of hepatic glucose production is gluconeogenesis, which is
427 under strict hormonal control. Silencing of HDAC4, 5 and 7 in mouse livers led to higher liver
428 glycogen content and improved glucose tolerance[59]. Mechanistically, the fasting hormone
429 glucagon promotes the dephosphorylation and nuclear shuttling of class IIa HDACs in HepG2
430 hepatocytes. In the nucleus, class IIa HDACs recruit HDAC3 to promoter regions of
431 gluconeogenic genes to enable the deacetylation of the FOXO transcription factor and the
432 induction of downstream genes, including *G6pc* that encodes glucose-6-phosphatase, a key
433 enzyme mediating gluconeogenesis[59]. An analogous pathway of hormone-activated
434 HDAC4/FOXO regulation of glucose and lipid metabolism was also identified in *Drosophila*
435 *melanogaster*[60]. Given these studies, it is possible that myeloid HDAC7 also contributes to
436 hyperglycaemia via activating gluconeogenic genes downstream of glucagon signalling.
437
438 Liver inflammation in MacHDAC7 and MacBlue mice on the HFHCHS was comparable
439 (**Figure 3F-G**), in contrast to the increased inflammation in MacHDAC7 mice on a chow diet
440 (**Figure 3A-G**). The lack of an enhanced inflammatory phenotype in obese MacHDAC7 mice
441 may reflect that HDAC7 overexpression could share some features of diet-induced
442 inflammation. In contrast, levels of inflammatory mediators were not significantly reduced in
443 the livers or plasma of myeloid *Hdac7*$^{-/-}$ mice fed a HFHCHS diet (**Figure S3-S4**), although
444 BMMs isolated from these mice on a chow diet showed reduced production of inflammatory
445 mediators (**Figure S3B**, right side of graphs). The lack of an obesity-driven inflammatory
446 phenotype in myeloid *Hdac7*$^{-/-}$ mice may reflect compensatory effect of other class IIa HDACs,

447 as previously observed in activated macrophages *in vitro*[30]. It may also reflect variability in
448 efficiency and/or specificity of the LysM-Cre system for conditional gene deletion in myeloid
449 cells[61], as highlighted by a previous study examining immune and non-immune cell populations
450 of the lung[62]. Alternatively, myeloid HDAC7 may have distinct roles in obesity- versus LPS-
451 driven inflammation. We previously showed that HDAC7 promotes glycolysis and associated
452 IL-1β production in macrophages responding to LPS[30]. However, during bacterial infection,
453 macrophage HDAC7 engages the pentose phosphate pathway to generate the metabolite
454 ribulose-5-phosphate that suppresses macrophage inflammatory responses[40]. This context-
455 dependent role of myeloid HDAC7 in controlling macrophage inflammatory responses makes
456 it difficult to predict its functions in different inflammation-driven conditions. Nonetheless,
457 taken together with the pronounced effects of myeloid gain-of-function HDAC7 in
458 exacerbating hepatic inflammation (**Figure 1, 3**), the subtle reduction in phenotypes associated
459 with MASLD in myeloid *Hdac7*$^{-/-}$ mice (**Figure S4**) is suggestive of a potential role for
460 HDAC7 in contributing to hepatic inflammation during metabolic dysfunction. The
461 involvement of myeloid HDAC7 in glucose dysregulation, as demonstrated through both gain-
462 of-function (**Figure 4**) and loss-of-function (**Figure 5**) models, is consistent with such a link.
463
464 In conclusion, this study has identified an association between myeloid HDAC7 and both
465 hepatic and systemic glucose metabolism, thus identifying a potential role for macrophage-
466 expressed HDAC7 in controlling whole body metabolism. This lysine deacetylase and
467 scaffolding protein likely promotes the breakdown of liver glycogen, which may partly explain
468 HDAC7-mediated hyperglycaemia during obesity. Future studies should address molecular
469 mechanisms by which HDAC7 mediates glycogenolysis and systemic glucose dysregulation.
470 Myeloid HDAC7 overexpression also increased hepatic inflammation in mice under a chow
471 diet, but an important limitation of our study is that we did not identify the mechanisms
472 involved. Nonetheless, our findings are consistent with the known role of HDAC7 in driving
473 both PKM2-mediated inflammatory responses[30, 39, 63] and oxidative stress[40] in macrophages. In
474 contrast, although myeloid *Hdac7* deletion improved glucose regulation under HFHCHS, it did
475 not reduce hepatic inflammation. Thus, endogenous HDAC7 is not essential for driving diet-
476 induced liver inflammation. Nonetheless, *HDAC7* expression was elevated in liver biopsies of
477 people with advanced versus early CLD (**Figure 6A**) and in tumours derived from a mouse
478 liver carcinoma model[64], with myeloid HDAC7 directing expression of genes associated with
479 advanced CLD in human (**Figure 6B-F**). Thus, it will be of interest in the future to evaluate
480 whether small molecule inhibitors of class IIa HDACs[65, 66] can attenuate dysregulated

481 metabolism, chronic inflammation and/or liver fibrosis in mouse models of obesity-driven
482 CLD.

483 ## Materials and methods

484 **Ethics statement**

485 All animal studies were approved by The University of Queensland Animal Ethics Committee.
486 Experimental procedures followed the approved projects 2021/AE00629, 2021/AE00630 and
487 2021/AE001048. Mice were bred and housed on a 12 h-controlled day/night cycle with food
488 and water available ad libitum in the Queensland Biosciences Precinct animal house (Institute
489 for Molecular Bioscience, The University of Queensland). Mice were monitored during
490 experiments in accordance with protocols approved in the above animal ethics certificates.

491

492 **Animals**

493 6-10 wk old male MacHDAC7 mice and control MacBlue mice (total of n=14-15 per group)
494 were fed a HFHCHS diet containing 20% kcal fat, 20 g/kg cholesterol, 222 g/kg fructose and
495 107 g/kg sucrose (Specialty Feeds, SF21-160, containing sodium caseinate) for 24 wk. The
496 control groups (n=3 per genotype) were fed a chow diet for the same time. These experiments
497 were carried out as two independent trials. Alternatively, 8-12 wk old male *Hdac7*$^{-/-}$ and wild
498 type control *Hdac7*$^{+/+}$ mice (n=12 per genotype) were fed a HFHCHS diet (Specialty Feeds,
499 SF18-074, same nutrient composition to SF21-160 except that it contains casein) for 36 wk.
500 Body weight was measured weekly throughout the trials. Fat and lean mass was measured
501 using a Minispec LF50 NMR Analyser (Bruker) one week before the end of the study. At the
502 termination of the study, mice were fasted for 6 or 12 h before being euthanised with isoflurane.
503 Blood was collected via cardiac puncture followed by perfusion with 0.9% saline solution
504 (Baxter). Liver, spleen, kidney and epididymal white adipose tissue were collected, weighed,
505 snap frozen, then fixed in 10% neutral buffered formalin or processed for RNA extraction.
506 Relative tissue weight gain for mice of each genotype was calculated by normalizing each
507 HFHCHS-fed mouse to the mean chow-fed tissue weight using the formula: [(HFHCHS tissue
508 weight − chow mean)/chow mean] × 100%.

509

510 **Fasted glucose measurements**

511 Mice were fasted for 6 h before blood was collected at midday from the saphenous or tail vein
512 using an EDTA-coated collection tube every 4 wk. Glucose levels were measured immediately
513 after the puncture with an Accu-Check Aviva Nano glucose meter (Roche).

514

515 **Glucose and insulin tolerance tests**

516 Mice were fasted for 6 h and blood glucose levels were measured from the tail vein before
517 intraperitoneal injection. For glucose tolerance tests, MacHDAC7 and MacBlue mice were
518 injected with 2 g/kg of D-glucose (AJAX), whereas *Hdac7*$^{-/-}$ and *Hdac7*$^{+/+}$ mice were injected
519 with 1g/kg of glucose. For insulin tolerance tests, *Hdac7*$^{-/-}$ and *Hdac7*$^{+/+}$ mice were fasted for
520 6 h before being injected with 0.75 U/kg insulin (NovoRapid). Blood glucose levels were
521 measured from the tail vein at the indicated time points with an Accu-Check Aviva Nano
522 glucose meter (Roche). For the tests on MacHDAC7 and MacBlue mice, data were combined
523 from two independent experiments.

524

525 **Histological assessment**

526 Formalin-fixed mouse livers were processed for paraffin-embedded histology for Hematoxylin
527 and Eosin (H&E) and Sirius Red staining. Unstained slides were processed for H&E staining
528 using a DAKO autostainer. Sirius Red slides were processed using the Llewellyn modification
529 of the Sirius Red technique[67]. In short, slides were stained with haematoxylin and then treated
530 with Sirius Red solution for 1 h before washing in tap water for 10 min. Slides were imaged
531 using a clinical microscope (BX43 or BX51, Olympus). Livers were scored using the NASH
532 Clinical research Network (NASH-CRN) scoring system[68]. In this method, scores for steatosis,
533 ballooning and lobular inflammation are summed to generate an overall score for likelihood of
534 steatohepatitis.

535

536 **Immune profiling**

537 MacBlue and MacHDAC7 mice, either at end-point of the chow diet versus HFHCHS diet trial
538 (24 weeks: 30-34 weeks of age) or at 6 to 10 weeks of age, were anesthetized with isofluorane
539 and 0.5-1 mL of blood was collected into heparinised tubes by cardiac puncture before cervical
540 dislocation. Spleens were collected and processed as previously described[69]. In brief, spleens
541 were weighed and then dissociated in 3 mL PBS 2% NCS 2 mM EDTA using a GentleMACS
542 Dissociator tissue homogenizer with matching C tubes (Miltenyi Biotec, Macquarie Park,
543 Australia) on "spleen 3" setting, twice. Spleen cells were counted either diluted 1:2 on a Coulter
544 Counter (Beckman Coulter) or neat on a Mindray BC-5000 Vet Auto hematology analyser
545 (Biomedical Electronics Co. LTD., China). Blood was counted neat on a Mindray BC-5000 Vet
546 Auto hematology analyser. For immunophenotyping, spleen samples were stained in 50%
547 CD16/CD32 hybridoma 2.4G2 supernatant for blocking and a fluorescent antibody cocktail
548 containing anti-mouse CD45-Pacific Blue (BioLegend, Cat#103126, clone 30-F11, 1/200

549 dilution), anti-mouse CD3ε-FITC (BioLegend, cat# 100306, clone 145-2C11, 1/200 dilution),
550 anti-mouse/human B220-APC-Cy7 (BioLegend, cat# 03224, clone RA3-6B2, 1/200 dilution)
551 and anti-mouse/human CD11b-PerCP-Cy5.5 (BioLegend, cat# 101228, clone M1/70, 1/200
552 dilution) was used to measure numbers of T, B and total myeloid cells. 7-amino-actinomycin
553 D (7AAD; ThermoFisher Scientific, cat# A1310, 1/10 dilution) or fixable viability stain
554 (FVS)700 (BD Bioscience, cat# 564997, 1/10,000 dilution) was added to all stained samples
555 for dead cell exclusion. Samples were analyzed on a Cytoflex (Beckman Coulter) flow
556 cytometer equipped with 640 nm, 561 nm, 488 nm and 405 nm lasers. Uncompensated FCS
557 files were analyzed using FlowJo 10.10 software, following compensation with single color
558 antibody stains (Tree Star, Ashland, OR) and following post-hoc compensation with single
559 color controls. The gating strategy used for flow cytometry analysis is shown in **Figure S5**.
560

561 **Glycogen quantification**

562 The method used was previously described[70, 71]. Snap-frozen mouse livers were homogenised
563 in 1 mL isolation buffer (50 mM Tris, pH 8, 150 mM NaCl, 2 mM EDTA, 50 mM NaF, 5 mM
564 sodium pyrophosphate, Sigma-Aldrich). 20 µL homogenate was then digested in 22.5 µL
565 acetate mix (1:8 mixture of 10% acetic acid (Sigma-Aldrich):200 mM sodium acetate buffer
566 (Sigma-Aldrich) (pH4.5)) with 5 µL and amyloglucosidase ~3260 U/mL, Megazyme) at 50 °C
567 for 30 min. The same amount of undigested liver homogenates boiled for 10 min was used for
568 correcting background glucose levels. Liver homogenates were then centrifuged at 20,000 *g*
569 for 10 min and transferred to a 96-well plate. Serially diluted D-glucose was used for generating
570 the calibration curve. 30 µL samples were then mixed with a reaction mix containing 150 µL
571 of 200 mM tricine/KOH (pH 8) (Sigma-Aldrich) and 10 mM MgCl2 (Sigma-Aldrich), 1 µL of
572 112.5 mM NADP (NADP), 1 µL of 180 mM of ATP (NADP) and 0.5 µL glucose-6-phosphate
573 dehydrogenase (Roche) to a volume of 200 µL. Absorbance at 340 nm was recorded for 20 min
574 before as well as 30 min after the addition of hexokinase (Roche). Glycogen content was
575 corrected for the weight of homogenised liver tissues.
576

577 **Insulin measurements**

578 Blood collected from saphenous vein or by cardiac puncture was centrifuged at 10,000 rpm for
579 10 min. Concentrations of insulin in mouse serum or plasma were measured using a mouse
580 insulin ELISA kit (Crystal Chem Mouse Insulin ELISA Kit, 90080), following the
581 manufacturer's instruction. Standard solutions and samples were added in duplicate into the
582 wells included in the kits and incubated for 2 h at 4 °C . Each well was then washed thoroughly.

583 Next, enzyme conjugate solution was added and incubated for 30 min at room temperature,
584 followed by another washing step. Enzyme substrate solution was immediately added and
585 incubated for 40 mi at room temperature in the dark. Following that, enzyme stop solution was
586 added to each well to stop the reaction. Finally, the absorbance at A450 and A630 was measured
587 using a microplate reader. Sample insulin concentrations were calculated based on a standard
588 curve generated using known insulin concentrations from the standard solutions included in
589 the kits.
590
591 **Cell culture**
592 Bone marrow cells were collected from femurs and tibias of mice and cultured in RPMI media
593 supplemented with 10% FBS, 2mM L-glutamine, 50 U/mL penicillin and 50 μg/mL
594 streptomycin (Gibco) in the presence of 150 ng/mL recombinant human macrophage colony-
595 stimulating factor-1 (Protein Expression Facility, UQ) for 6 days. Differentiated BMMs were
596 harvested in DPBS (Thermo Fisher Scientific) and resuspended in culture media for stimulation
597 with indicated concentrations of LPS (*Salmonella enterica* serotype Minnesota, L2137, Sigma-
598 Aldrich). To induce IL-1β processing and secretion, 5 μg/mL nigericin (N7143, Sigma-Aldrich)
599 was added to cells 1 h prior to harvesting culture supernatants. Cell culture supernatants were
600 then collected, centrifuged at 1,000 *g* for 5 min and stored at -80 °C until analysis.
601
602 **Cytokine profiling**
603 Cell culture supernatants and mouse plasma were diluted in culture media and DPBS,
604 respectively. CCL2 and IL-1β concentrations were measured using MCP-1/CCL2 Mouse
605 Uncoated ELISA and IL-1beta Mouse Uncoated ELISA Kits (mouse CCL2: 88-7391-77,
606 mouse IL-1β: 88-7013-77, Invitrogen) or with a Mouse CCL2/JE/MCP-1 DuoSet ELISA kit
607 (DY479, R&D SYSTEMS), as per the manufacturer's manuals.
608
609 **Quantification of gene expression**
610 To extract RNA from mouse livers, fresh tissues were frozen in lysis buffer from an ISOLATE
611 II RNA Mini kit (BioLine) at -80 °C. Snap-frozen tissues from naïve mice were homogenised
612 in lysis buffer. RNA purification was performed following the manufacturer's instructions. An
613 off-column DNA digestion was performed using DNAse I (Invitrogen), as per manufacturer's
614 instructions. RNA was reverse transcribed to cDNA using oligo dT and SuperScript III Reverse
615 Transcriptase (Invitrogen). Quantitative PCR (qPCR) was performed in 384-well plates using
616 cDNAs, SYBR Green PCR Master Mix (Applied Biosystem), and a ViiATM 7 Real-Time PCR

617 System (Applied Biosystems). mRNA levels of individual genes, relative to the housekeeping
618 gene hypoxanthine phosphoribosyl transferase (*Hprt*), were calculated using the ΔCt method[72].
619 Sequences of primers used for qPCR are listed in **Table S2**.
620
621 **Western blotting**
622 Differentiated BMMs were washed once with DPBS and lysed in RIPA buffer (50 mM Tris-
623 HCl, 150 mM NaCl, 0.1% SDS, 1% Sodium deoxycholate, 1% NP-40) supplemented with
624 protease inhibitor cocktail (cOmpleteTM, Roche) and phosphatase inhibitors (PhosStopTM,
625 Roche). Cell lysates were homogenised by passing through a 27G needle. Equal amounts of
626 homogenates were boiled and subjected to electrophoresis using pre-cast 4-12% Bis-Tris
627 NuPAGE gels in NuPAGE MOPS SDS running buffer (Invitrogen). After separation, proteins
628 were transferred to a nitrocellulose membrane and immunoblotted for endogenous HDAC7
629 using an anti-HDAC7 antibody (Cell Signaling Technology, 1/1000) followed by an HRP-
630 conjugated goat anti-rabbit IgG (Cell Signaling Technology, 0.026 µg/mL) and Tubulin as a
631 loading control using a fluorescent Rhodamine anti-Tubulin antibody (Bio-Rad, 1/5000).
632
633 **Quantification of hepatic *HDAC7* mRNA levels in human CLD**
634 Hepatic *HDAC7* mRNA levels were quantified in a cohort of 69 people with CLD of mixed
635 aetiologies. Diagnosis, disease scoring and sample stratification has previously been
636 described[51]. *HDAC7* mRNA levels in people with early (stages 0-2) and advanced (stages 3-4)
637 CLD were quantified by RNA sequencing, as previously described[51]. In brief, sequencing reads
638 were mapped to the human hg19 genome using STAR aligner[73] and CPM values of transcript
639 reads were obtained using the edgeR package[74]. Genes were filtered with a CPM threshold of
640 over 10 in at least 20 samples and subjected to normalisation using the Trimmed Mean of M-
641 values method using edgeR[75]. Differential gene expression was then analysed by likelihood-
642 ratio test, with multiple testing performed using Benjamini-Hochberg corrections[76]. FDR
643 values of less than 0.05 were considered significantly different.
644
645 **Spatial transcriptomics analyses**
646 Liver tissues were harvested from two male MacBlue and two male MacHDAC7 mice and
647 immediately fixed in 4% paraformaldehyde for 24 h at 4°C. Fixed tissues were processed,
648 embedded in paraffin, and sectioned at 5 µm thickness. Sections were mounted onto Xenium
649 V1 slides (10x Genomics) and processed according to the manufacturer's protocol for Xenium
650 Prime In Situ Gene Expression with Cell Segmentation Staining (10x Genomics, CG000760

651 RevC). Briefly, slides underwent deparaffinization and decrosslinking, followed by priming
652 hybridization, RNase treatment and polishing. The Xenium 5K Ms PTP Panel Probes (10x
653 Genomics, Cat#2001227), as well as an add-on custom probe panel targeting 50 genes,
654 including key macrophage, inflammatory, metabolic, and fibrosis-associated transcripts (**Table**
655 **S3**), was hybridised to the tissue sections overnight. Following probe ligation, rolling circle
656 amplification and cell segmentation staining steps, slides were loaded onto Xenium Analyzer
657 for signal detection and image acquisition. Raw image data were processed using the Xenium
658 Onboard Analysis pipeline, and decoded transcripts were mapped back to the tissue at the single
659 cell level. Data were analysed using Seurat workflow (Seurat version 5.1.0), including quality
660 control filtering, and gene expression quantification in R (version 4.4.0). EdgeR (version 4.4.0)
661 was used to perform differential gene expression analysis on MacBlue versus MacHDAC7
662 hepatic cells that were positive for both *eCFP* and *Hdac7* mRNAs and the results were
663 visualised on a heatmap. Genes overlapping with previously published CLD-associated
664 signatures were further examined for spatial co-localisation with bivariate Moran's Index (from
665 esda package version 2.2.1) using custom python scripts and were visualised with spatial
666 feature plots.
667
668 **Statistical analyses**
669 Data from *in vivo* experiments are combined from one or two independent trials with each
670 individual mouse representing one independent data point. For cell culture experiments, means
671 of experimental replicates were determined, with data from independent mice or experiments
672 being combined for statistical analysis. Statistical analyses were performed using Prism 9 or
673 10 (GraphPad). Comparisons between two groups were performed using a two-tailed unpaired
674 Student's *t*-test or Mann Whitney U test as indicated. For datasets involving at least three
675 variables, linear regression, ordinary or repeated measures two-way ANOVA tests were
676 performed followed by multiple comparisons, as indicated in individual figure legends.
677 Differences with confidence value of 95% and above ($p < 0.05$) were considered statistically
678 significant.

Acknowledgements

This work was supported by a National Health and Medical Research Council of Australia (NHMRC) Ideas grant (1184885 to MJS and DR), an NHMRC Investigator grant to MJS (1194406), and an Australian Infectious Disease Research Centre seed grant to CRE, MJS, JAE and DR. DK was supported by an Institute for Molecular Bioscience (IMB) Fellowship and an NHMRC Ideas grant (2012772). DPF was supported by an NHMRC Investigator grant (2009551) and an ARC Centre of Excellence grant (CE200100012). SSB was supported by a Swiss National Science Foundation Postdoc Mobility Fellowship (P2BEP3_191800) and a Novartis Foundation for Medical-Biological Research Fellowship (21C133). KMI was supported by an NHMRC Ideas grant (2012793).

Author contributions

Conceptualisation, Y.W., M.A.S., M.J.S., D.K.; Methodology, G.C.M., S.K., K.S.G., Z.L., S.S.B., K.M.I; Investigation, Y.W., D.R., K.D.G., P.P., K.B., G.C.M., Z.X., Yu.W., E.N.T., J.E.B.C., R.A., K.S.G., J.D.A., D.K.; Resources, G.C.M., J.A.E., C.R.E, A.D.C., E.E.P., J-P.L., Q.N.; Writing- original draft, Y.W., M.J.S., D.K.; Writing- Review/Writing, Y.W., G.C.M., P.P., S.S.B., D.P.F., K.M.I., M.A.S., M.J.S., D.K.; Supervision, K.S., D.P.F., A.D.C., K.M.I., M.A.S., J-P.L., Q.N., M.J.S., D.K.; Funding acquisition, D.R., C.R.E, J.A.E., M.J.S.

Conflict of Interest Statement

The authors claim no conflict of interest.

References

1. Huang DQ, Terrault NA, Tacke F, *et al.* Global epidemiology of cirrhosis - aetiology, trends and predictions. *Nat Rev Gastroenterol Hepatol* 2023; **20**: 388-398.
2. Moon AM, Singal AG, Tapper EB. Contemporary Epidemiology of Chronic Liver Disease and Cirrhosis. *Clin Gastroenterol Hepatol* 2020; **18**: 2650-2666.
3. Mitra S, De A, Chowdhury A. Epidemiology of non-alcoholic and alcoholic fatty liver diseases. *Transl Gastroenterol Hepatol* 2020; **5**: 16.
4. Keam SJ. Resmetirom: First Approval. *Drugs* 2024; **84**: 729-735.
5. Bansal MB, Patton H, Morgan TR, Carr RM, Dranoff JA, Allen AM. Semaglutide therapy for metabolic dysfunction-associated steatohepatitis: November 2025 updates to AASLD Practice Guidance. *Hepatology* 2025; doi: 10.1097/HEP.0000000000001608.
6. Do A, Zahrawi F, Mehal WZ. Therapeutic landscape of metabolic dysfunction-associated steatohepatitis (MASH). *Nat Rev Drug Discov* 2025; **24**: 171-189.
7. Loomba R, Hartman ML, Lawitz EJ, *et al.* Tirzepatide for Metabolic Dysfunction-Associated Steatohepatitis with Liver Fibrosis. *N Engl J Med* 2024; **391**: 299-310.
8. Mosser DM, Edwards JP. Exploring the full spectrum of macrophage activation. *Nat Rev Immunol* 2008; **8**: 958-969.
9. Davies LC, Jenkins SJ, Allen JE, Taylor PR. Tissue-resident macrophages. *Nat Immunol* 2013; **14**: 986-995.
10. Nguyen-Lefebvre AT, Horuzsko A. Kupffer Cell Metabolism and Function. *J Enzymol Metab* 2015; **1**: 101.
11. Dixon LJ, Barnes M, Tang H, Pritchard MT, Nagy LE. Kupffer cells in the liver. *Compr Physiol* 2013; **3**: 785-797.
12. Tosello-Trampont AC, Landes SG, Nguyen V, Novobrantseva TI, Hahn YS. Kuppfer cells trigger nonalcoholic steatohepatitis development in diet-induced mouse model through tumor necrosis factor-alpha production. *J Biol Chem* 2012; **287**: 40161-40172.
13. Murray PJ, Wynn TA. Protective and pathogenic functions of macrophage subsets. *Nat Rev Immunol* 2011; **11**: 723-737.
14. Ramachandran P, Pellicoro A, Vernon MA, *et al.* Differential Ly-6C expression identifies the recruited macrophage phenotype, which orchestrates the regression of murine liver fibrosis. *Proc Natl Acad Sci U S A* 2012; **109**: E3186-3195.
15. Obstfeld AE, Sugaru E, Thearle M, *et al.* C-C chemokine receptor 2 (CCR2) regulates the hepatic recruitment of myeloid cells that promote obesity-induced hepatic steatosis. *Diabetes* 2010; **59**: 916-925.
16. Rivera CA, Adegboyega P, van Rooijen N, Tagalicud A, Allman M, Wallace M. Toll-like receptor-4 signaling and Kupffer cells play pivotal roles in the pathogenesis of non-alcoholic steatohepatitis. *J Hepatol* 2007; **47**: 571-579.
17. Braunersreuther V, Viviani GL, Mach F, Montecucco F. Role of cytokines and chemokines in non-alcoholic fatty liver disease. *World J Gastroenterol* 2012; **18**: 727-735.
18. Rull A, Rodriguez F, Aragones G, *et al.* Hepatic monocyte chemoattractant protein-1 is upregulated by dietary cholesterol and contributes to liver steatosis. *Cytokine* 2009; **48**: 273-279.
19. Haukeland JW, Damas JK, Konopski Z, *et al.* Systemic inflammation in nonalcoholic fatty liver disease is characterized by elevated levels of CCL2. *J Hepatol* 2006; **44**: 1167-1174.
20. Wree A, McGeough MD, Pena CA, *et al.* NLRP3 inflammasome activation is required for fibrosis development in NAFLD. *J Mol Med (Berl)* 2014; **92**: 1069-1082.
21. Negrin KA, Roth Flach RJ, DiStefano MT, *et al.* IL-1 signaling in obesity-induced hepatic lipogenesis and steatosis. *PLoS One* 2014; **9**: e107265.

22. Kamari Y, Shaish A, Vax E, *et al.* Lack of interleukin-1alpha or interleukin-1beta inhibits transformation of steatosis to steatohepatitis and liver fibrosis in hypercholesterolemic mice. *J Hepatol* 2011; **55**: 1086-1094.
23. Tandon P, Abrams ND, Carrick DM, *et al.* Metabolic Regulation of Inflammation and Its Resolution: Current Status, Clinical Needs, Challenges, and Opportunities. *J Immunol* 2021; **207**: 2625-2630.
24. O'Neill LA, Kishton RJ, Rathmell J. A guide to immunometabolism for immunologists. *Nat Rev Immunol* 2016; **16**: 553-565.
25. Lauterbach MA, Hanke JE, Serefidou M, *et al.* Toll-like Receptor Signaling Rewires Macrophage Metabolism and Promotes Histone Acetylation via ATP-Citrate Lyase. *Immunity* 2019; **51**: 997-1011 e1017.
26. Langston PK, Nambu A, Jung J, *et al.* Glycerol phosphate shuttle enzyme GPD2 regulates macrophage inflammatory responses. *Nat Immunol* 2019; **20**: 1186-1195.
27. Meoli L, Gupta NK, Saeidi N, *et al.* Nonalcoholic fatty liver disease and gastric bypass surgery regulate serum and hepatic levels of pyruvate kinase isoenzyme M2. *Am J Physiol Endocrinol Metab* 2018; **315**: E613-E621.
28. Xu F, Guo M, Huang W, *et al.* Annexin A5 regulates hepatic macrophage polarization via directly targeting PKM2 and ameliorates NASH. *Redox Biol* 2020; **36**: 101634.
29. Kong Q, Li N, Cheng H, *et al.* HSPA12A Is a Novel Player in Nonalcoholic Steatohepatitis via Promoting Nuclear PKM2-Mediated M1 Macrophage Polarization. *Diabetes* 2019; **68**: 361-376.
30. Das Gupta K, Shakespear MR, Curson JEB, *et al.* Class IIa Histone Deacetylases Drive Toll-like Receptor-Inducible Glycolysis and Macrophage Inflammatory Responses via Pyruvate Kinase M2. *Cell Rep* 2020; **30**: 2712-2728 e2718.
31. Park SY, Kim JS. A short guide to histone deacetylases including recent progress on class II enzymes. *Exp Mol Med* 2020; **52**: 204-212.
32. Narita T, Weinert BT, Choudhary C. Functions and mechanisms of non-histone protein acetylation. *Nat Rev Mol Cell Biol* 2019; **20**: 156-174.
33. Friedmann DR, Marmorstein R. Structure and mechanism of non-histone protein acetyltransferase enzymes. *FEBS J* 2013; **280**: 5570-5581.
34. Martin M, Kettmann R, Dequiedt F. Class IIa histone deacetylases: regulating the regulators. *Oncogene* 2007; **26**: 5450-5467.
35. Das Gupta K, Shakespear MR, Iyer A, Fairlie DP, Sweet MJ. Histone deacetylases in monocyte/macrophage development, activation and metabolism: refining HDAC targets for inflammatory and infectious diseases. *Clin Transl Immunology* 2016; **5**: e62.
36. Shakespear MR, Halili MA, Irvine KM, Fairlie DP, Sweet MJ. Histone deacetylases as regulators of inflammation and immunity. *Trends Immunol* 2011; **32**: 335-343.
37. Wang Y, Abrol R, Mak JYW, *et al.* Histone deacetylase 7: a signalling hub controlling development, inflammation, metabolism and disease. *FEBS J* 2023; **290**: 2805-2832.
38. Kodikara IKM, Pflum MKH. Scaffolding Activities of Pseudodeacetylase HDAC7. *ACS Chem Biol* 2025; **20**: 248-258.
39. Ramnath D, Das Gupta K, Wang Y, *et al.* The histone deacetylase Hdac7 supports LPS-inducible glycolysis and Il-1beta production in murine macrophages via distinct mechanisms. *J Leukoc Biol* 2022; **111**: 327-336.
40. Das Gupta K, Ramnath D, von Pein JB, *et al.* HDAC7 is an immunometabolic switch triaging danger signals for engagement of antimicrobial versus inflammatory responses in macrophages. *Proc Natl Acad Sci U S A* 2023; **120**: e2212813120.
41. Shakespear MR, Hohenhaus DM, Kelly GM, *et al.* Histone deacetylase 7 promotes Toll-like receptor 4-dependent proinflammatory gene expression in macrophages. *J Biol Chem* 2013; **288**: 25362-25374.

42. Ovchinnikov DA, van Zuylen WJ, DeBats CE, Alexander KA, Kellie S, Hume DA. Expression of Gal4-dependent transgenes in cells of the mononuclear phagocyte system labeled with enhanced cyan fluorescent protein using Csf1r-Gal4VP16/UAS-ECFP double-transgenic mice. *J Leukoc Biol* 2008; **83**: 430-433.
43. Baeck C, Wehr A, Karlmark KR*, et al.* Pharmacological inhibition of the chemokine CCL2 (MCP-1) diminishes liver macrophage infiltration and steatohepatitis in chronic hepatic injury. *Gut* 2012; **61**: 416-426.
44. Parker R, Weston CJ, Miao Z*, et al.* CC chemokine receptor 2 promotes recruitment of myeloid cells associated with insulin resistance in nonalcoholic fatty liver disease. *Am J Physiol Gastrointest Liver Physiol* 2018; **314**: G483-G493.
45. Kitade H, Chen G, Ni Y, Ota T. Nonalcoholic Fatty Liver Disease and Insulin Resistance: New Insights and Potential New Treatments. *Nutrients* 2017; **9**: 387.
46. Sharabi K, Tavares CD, Rines AK, Puigserver P. Molecular pathophysiology of hepatic glucose production. *Mol Aspects Med* 2015; **46**: 21-33.
47. Hatting M, Tavares CDJ, Sharabi K, Rines AK, Puigserver P. Insulin regulation of gluconeogenesis. *Ann N Y Acad Sci* 2018; **1411**: 21-35.
48. Rull A, Escola-Gil JC, Julve J*, et al.* Deficiency in monocyte chemoattractant protein-1 modifies lipid and glucose metabolism. *Exp Mol Pathol* 2007; **83**: 361-366.
49. Kanda H, Tateya S, Tamori Y*, et al.* MCP-1 contributes to macrophage infiltration into adipose tissue, insulin resistance, and hepatic steatosis in obesity. *J Clin Invest* 2006; **116**: 1494-1505.
50. Petersen MC, Vatner DF, Shulman GI. Regulation of hepatic glucose metabolism in health and disease. *Nat Rev Endocrinol* 2017; **13**: 572-587.
51. Ramnath D, Irvine KM, Lukowski SW*, et al.* Hepatic expression profiling identifies steatosis-independent and steatosis-driven advanced fibrosis genes. *JCI Insight* 2018; **3**: e120274.
52. Gwag T, Reddy Mooli RG, Li D, Lee S, Lee EY, Wang S. Macrophage-derived thrombospondin 1 promotes obesity-associated non-alcoholic fatty liver disease. *JHEP Rep* 2021; **3**: 100193.
53. Hamada T, Fondevila C, Busuttil RW, Coito AJ. Metalloproteinase-9 deficiency protects against hepatic ischemia/reperfusion injury. *Hepatology* 2008; **47**: 186-198.
54. Kim YS, Nam HJ, Han CY*, et al.* Liver X Receptor Alpha Activation Inhibits Autophagy and Lipophagy in Hepatocytes by Dysregulating Autophagy-Related 4B Cysteine Peptidase and Rab-8B, Reducing Mitochondrial Fuel Oxidation. *Hepatology* 2021; **73**: 1307-1326.
55. Han HS, Kang G, Kim JS, Choi BH, Koo SH. Regulation of glucose metabolism from a liver-centric perspective. *Exp Mol Med* 2016; **48**: e218.
56. Agius L. Role of glycogen phosphorylase in liver glycogen metabolism. *Mol Aspects Med* 2015; **46**: 34-45.
57. Zhang T, Wang S, Lin Y*, et al.* Acetylation negatively regulates glycogen phosphorylase by recruiting protein phosphatase 1. *Cell Metab* 2012; **15**: 75-87.
58. Ma J, Wei K, Liu J*, et al.* Glycogen metabolism regulates macrophage-mediated acute inflammatory responses. *Nat Commun* 2020; **11**: 1769.
59. Mihaylova MM, Vasquez DS, Ravnskjaer K*, et al.* Class IIa histone deacetylases are hormone-activated regulators of FOXO and mammalian glucose homeostasis. *Cell* 2011; **145**: 607-621.
60. Wang B, Moya N, Niessen S*, et al.* A hormone-dependent module regulating energy balance. *Cell* 2011; **145**: 596-606.

847 61. Hume DA. Applications of myeloid-specific promoters in transgenic mice support in
848 vivo imaging and functional genomics but do not support the concept of distinct macrophage
849 and dendritic cell lineages or roles in immunity. *J Leukoc Biol* 2011; **89**: 525-538.
850 62. McCubbrey AL, Allison KC, Lee-Sherick AB, Jakubzick CV, Janssen WJ. Promoter
851 Specificity and Efficacy in Conditional and Inducible Transgenic Targeting of Lung
852 Macrophages. *Front Immunol* 2017; **8**: 1618.
853 63. Kadier K, Niu T, Ding B*, et al.* PROTAC-Mediated HDAC7 Protein Degradation
854 Unveils Its Deacetylase-Independent Proinflammatory Function in Macrophages. *Adv Sci*
855 *(Weinh)* 2024; **11**: e2309459.
856 64. Freese K, Seitz T, Dietrich P*, et al.* Histone Deacetylase Expressions in Hepatocellular
857 Carcinoma and Functional Effects of Histone Deacetylase Inhibitors on Liver Cancer Cells In
858 Vitro. *Cancers (Basel)* 2019; **11**: 1587.
859 65. Poon EK, Liu L, Wu KC*, et al.* A novel inhibitor of class IIa histone deacetylases
860 attenuates collagen-induced arthritis. *Br J Pharmacol* 2024; **181**: 4804-4821.
861 66. Guerriero JL, Sotayo A, Ponichtera HE*, et al.* Class IIa HDAC inhibition reduces breast
862 tumours and metastases through anti-tumour macrophages. *Nature* 2017; **543**: 428-432.
863 67. Llewellyn BD. An improved Sirius red method for amyloid. *J Med Lab Technol* 1970;
864 **27**: 308-309.
865 68. Kleiner DE, Brunt EM, Van Natta M*, et al.* Design and validation of a histological
866 scoring system for nonalcoholic fatty liver disease. *Hepatology* 2005; **41**: 1313-1321.
867 69. Bisht K, Tay J, Wellburn RN*, et al.* Bacterial Lipopolysaccharides Suppress
868 Erythroblastic Islands and Erythropoiesis in the Bone Marrow in an Extrinsic and G- CSF-, IL-
869 1-, and TNF-Independent Manner. *Front Immunol* 2020; **11**: 583550.
870 70. Wang Z, Liu Q, Wang L, Gilbert RG, Sullivan MA. The Extraction of Liver Glycogen
871 Molecules for Glycogen Structure Determination. *J Vis Exp* 2022; doi: 10.3791/63088.
872 71. Suzuki Y, Lanner C, Kim JH*, et al.* Insulin control of glycogen metabolism in knockout
873 mice lacking the muscle-specific protein phosphatase PP1G/RGL. *Mol Cell Biol* 2001; **21**:
874 2683-2694.
875 72. Livak KJ, Schmittgen TD. Analysis of relative gene expression data using real-time
876 quantitative PCR and the 2(-Delta Delta C(T)) Method. *Methods* 2001; **25**: 402-408.
877 73. Dobin A, Davis CA, Schlesinger F*, et al.* STAR: ultrafast universal RNA-seq aligner.
878 *Bioinformatics* 2013; **29**: 15-21.
879 74. Law CW, Chen Y, Shi W, Smyth GK. voom: Precision weights unlock linear model
880 analysis tools for RNA-seq read counts. *Genome Biol* 2014; **15**: R29.
881 75. Robinson MD, Oshlack A. A scaling normalization method for differential expression
882 analysis of RNA-seq data. *Genome Biol* 2010; **11**: R25.
883 76. Robinson MD, McCarthy DJ, Smyth GK. edgeR: a Bioconductor package for
884 differential expression analysis of digital gene expression data. *Bioinformatics* 2010; **26**: 139-
885 140.
886

887 # Tables

888 **Table 1. Haematological assessment of circulating immune cells in 30-34 week old**
889 **MacBlue and MacHDAC7 mice fed a chow or HFHCHS diet.**

	Chow		HFHCHS	
	MacBlue	**MacHDAC7**	**MacBlue**	**MacHDAC7**
WBC (10^9/L)	1.702 ± 0.252	1.783 ± 0.211	2.169 ± 0.303	1.835 ± 0.26
Neutrophil (10^9/L)	0.243 ± 0.032	0.725 ± 0.157[a]	0.519 ± 0.070	0.634 ± 0.123
Monocyte (10^9/L)	0.045 ± 0.007	0.062 ± 0.005	0.079 ± 0.009[b]	0.057 ± 0.008
Eosinophil (10^9/L)	0.027 ± 0.008	0.053 ± 0.014	0.031 ± 0.005	0.035 ± 0.008
Basophil (10^9/L)	0.003 ± 0.002	0.007 ± 0.003	0.005 ± 0.002	0.004 ± 0.002
Lymphoid (10^9/L)	1.383 ± 0.218	0.937 ± 0.28	1.535 ± 0.249	1.106 ± 0.187
RBC (10^{12}/L)	7.388 ± 0.946	7.93 ± 0.279	8.406 ± 0.239	8.187 ± 0.153
Platelet (10^9/L)	1128.833 ± 186.582	837.333 ± 168.627	906 ± 80.965	949.643 ± 52.093

890 Data shown are mean ± SEM and represent n =6 (chow) or n=14 (HFHCHS) mice for each genotype. Statistical
891 analyses were performed using two-way ANOVA followed by Fisher's LSD test.
892 [a]MacBlue vs MacHDAC7 fed a chow diet, p=0.0230
893 [b]Chow vs HFHCHS in MacBlue group, p=0.0208

894 **Table 2. Haematological assessment of circulating immune cells in 6-8 week old MacBlue**
895 **and MacHDAC7 mice**

	MacBlue	**MacHDAC7**
RBC (10^{12}/L)	8.143 ± 0.423	8.355 ± 0.224
WBC (10^{9}/L)	2.584 ± 0.270	6.337 ± 0.925**
Neutrophil (10^{9}/L)	0.434 ± 0.061	1.862 ± 0.997*
Monocyte (10^{9}/L)	0.274 ± 0.077	0.232 ± 0.071
Eosinophil (10^{9}/L)	0.214 ± 0.087	0.230 ± 0.062
Basophil (10^{9}/L)	0.002 ± 0.002	0.012 ± 0.002
Lymphocyte (10^{9}/L)	1.654 ± 0.136	4.002 ± 0.673
Platelet (10^{9}/L)	740.700 ± 107.900	539.000 ± 89.180
HGB (g/L)	125.600 ± 5.385	137.000 ± 3.958
HCT	0.376 ± 0.18	0.403 ± 0.014

896 HGB: Haemoglobin; HCT: Haematocrit. Data shown are mean ± SEM and represent n =7 for Macblue and n = 6
897 for MacHDAC7 for each group. Statistical analyses were performed using Mann-Whitney U test. * p <0.05; ** p
898 <0.01.

899 **Table 3. Assessment of spleen weight and immune cells in MacBlue and MacHDAC7**

	MacBlue	**MacHDAC7**
Spleen weight (mg)	73.000 ± 3.499	217.200 ± 19.760****
Splenocytes (10^6 cells/spleen)	86.210 ± 7.497	245.200 ± 27.79****
B220+ B cells (10^6 cells/spleen)	27.170 ± 2.957	70.270 ± 8.621****
CD3+ T cells (10^6 cells/spleen)	30.970 ± 4.840	47.800 ± 4.962*
CD11b+ Myeloid cells (10^6 cells/spleen)	12.860 ± 2.720	83.720 ± 20.100****

900 Data shown are mean ± SEM and represent n =10 for Macblue and n = 9 for MacHDAC7 for each group. Statistical
901 analyses were performed using Mann-Whitney U test. * p <0.05; **** p <0.0001.

902 ## Figure Legends:

903 **Figure 1. Myeloid *Hdac7* overexpression promotes expression of inflammatory genes in**
904 **the liver.**
905 mRNA levels of *Hdac7* (A), *Ccl2* (B), *Il1b* (C) and *Mmp9* (D) in livers from 9-22 wk old
906 MacHDAC7 and control MacBlue mice fed a chow diet. Data (normalised to *Hprt*) represent
907 mean ± SEM from n=12 mice (6 female and 6 male) for each group. Statistical significance
908 was determined by Student's *t*-test (ns, not significant; * p <0.05).
909

910 **Figure 2. Effect of myeloid *Hdac7* overexpression on body weight gain in mice fed a chow**
911 **versus HFHCHS diet.**
912 8-10 wk old male MacBlue and MacHDAC7 mice were fed a chow diet (chow, n=6 per group)
913 or a high fat, high cholesterol and high sucrose diet (HFHCHS, n=14-15 per group) for 24 wk.
914 A. Weekly body weight. B. Average weight gain in mice fed a HFHCHS versus chow diet,
915 calculated by substracting the average body weight of mice fed the chow diet from that of mice
916 fed the HFHCHS. Data shown are mean ± SEM of n=6 (chow) or n=14-15 (HFHCHS) mice
917 per group. Statistical analyses were perfomed using linear regression to compare the difference
918 in body weight between MacBlue and MacHDAC7 mice fed on their respective diets or
919 HFHCHS-induced weight gain (** p <0.01; **** p <0.0001). C. Fat and lean mass measured
920 by EchoMRI at wk 23. D-G. Tissue weights of liver, epididymal white adipose tissue (WAT),
921 kidney and spleen at wk 24. Data shown are mean ± SEM of n=6 (chow) or n=14 (HFHCHS)
922 mice and were analysed using repeated measures (C) or ordinary (D-G) two-way ANOVA
923 followed by Sidak's multiple comparison (ns, not significant; * p <0.05; ** p <0.01; **** p
924 <0.0001).
925

926 **Figure 3. Myeloid *Hdac7* overexpression drives hepatic inflammation but not steatosis.**
927 Hepatic mRNA levels of genes encoding inflammatory mediators and serum CCL2 levels in
928 male MacBlue and MacHDAC7 mice fed a chow or HFHCHS diet. A-B. Liver mRNA levels
929 of *Ccl2* (A) and *Il1b* (B) relative to *Hprt* were measured by RT-qPCR. C. CCL2 levels in mouse
930 serum were measured by ELISA. D-E. Liver mRNA levels of F4/80-encoding *Adgre1* (D) and
931 *Clec4f* (E) relative to *Hprt* were measured by RT-qPCR. F. Representative H&E staining of
932 livers from chow- or HFHCHS-fed MacBlue and MacHDAC7 mice. Photos were acquired at
933 40 x magnification, scale bar: 100 μm. Large lipid droplets (black arrows) and small lipid
934 droplets (blue arrows) and a focus of inflammation within the lobule (red arrows). G-I.

935 Quantification of lobular inflammation (G), lipid droplet counts (H-I), steatosis (J) and NAFLD
936 activity score (K), as per the NASH clinical research network scoring system after H&E
937 staining. Data represent mean ± SEM of n=6 (chow) or n=14 (HFHCHS) mice for each
938 treatment group and were analysed using two-way ANOVA followed by Fisher's LSD test (A-
939 E) or Sidak's multiple comparison (G-K) (ns, not significant; * $p< 0.05$; ** $p< 0.01$; *** $p<$
940 0.001; **** $p< 0.0001$).
941
942 **Figure 4. Myeloid *Hdac7* overexpression increases fasted blood glucose levels, glucose**
943 **dysregulation and glycogen metabolism in mice fed a HFHCHS diet.**
944 6 h fasted blood glucose levels of MacBlue and MacHDAC7 mice fed a chow (**A**) or HFHCHS
945 (**C**) diet. Glucose tolerance test (GTT) was performed at wk 12 (**B** and **D**). Data shown are
946 mean ± SEM of n=5-6 (chow) or n=15 (HFHCHS) mice for each group. AUC, area under curve
947 analysis. **E.** Liver glycogen quantification. At termination of the study, mice were fasted for 6
948 h and glycogen levels were quantified in snap-frozen livers. Data (mean ± SEM) represent n=6
949 (chow) or n=14 (HFHCHS) mice for each group. **F.** Insulin levels in the circulation. Circulating
950 insulin levels were measured before diet feeding (wk 0), at wk 4 and at end-point, after mice
951 were fasted for 6 h. Data are mean ± SEM of n=5-6 (chow) or n=14 (HFHCHS) mice for each
952 treatment group. Statistical analyses were performed using Student's *t*-test (**A-D, F** wk 0) or
953 two-way ANOVA followed by Sidak's multiple comparison (**B, D, E-F**) (ns, not significant; *
954 $p< 0.05$; ** $p< 0.01$; *** $p< 0.001$).
955
956 **Figure 5. Myeloid *Hdac7* deficiency reduced fasting blood glucose levels in mice fed a**
957 **HFHCHS diet.**
958 8-10 wk old male *Hdac7*$^{+/+}$ and *Hdac7*$^{-/-}$ mice were fed a HFHCHS diet for 36 wk. **A.** Fasted
959 blood glucose levels were measured at wk 0, 8, 14, 16 and 24. Data are mean ± SEM of n=12
960 mice for each group and were analysed using Student's *t*-test (ns, not significant; * $p < 0.05$;
961 **** $p < 0.0001$). Glucose tolerance test (GTT) at wk 14 and wk 32 (**B-C**) and insulin tolerance
962 test (ITT) at wk 19 and wk 34 (**D-E**). Data shown are mean ± SEM of n=12 mice/ group.
963 Statistical analyses were performed using repeated measures two-way ANOVA followed by
964 Sidak's multiple comparison. Area under curve (AUC) of GTTs and ITTs were analysed using
965 Student's *t*-test (ns, not significant; * $p < 0.05$; ** $p < 0.01$).
966
967 **Figure 6. Association of *HDAC7* mRNA expression with signatures of human CLD.**

968 **A.** mRNA levels of *HDAC7* in liver biopsies from patients with early (stages 0-2) versus
969 advanced (stages 3-4) of CLD was determined by RNAseq. Differentially expressed genes
970 were identified using edgeR with TMM normalisation and Benjamini-Hochberg method for fdr
971 correction. Data indicate mean ± SEM, n = 69 (circles = early stages and triangles = advanced
972 stages). **B-F.** Spatial transcriptomic profiling of liver tissues from MacBlue and MacHDAC7
973 mice was performed using the 10x Genomics Xenium platform. Expression of eCFP and
974 HDAC7 mRNAs was used to identify hepatic myeloid cells expressing HDAC7
975 (CFP^+/$HDAC7^+$ cells). **B.** A heatmap showing the 53 differentially expressed genes in
976 CFP^+/$HDAC7^+$ macrophages from MacBlue versus MacHDAC7 livers. **C-F.** Spatial co-
977 expression analysis of *VCAN* (**C**), *THBS1* (**D**), *MMP9* (**E**) and *RAB8B* (**F**) in MacBlue and
978 MacHDAC7 livers. Data are representative of two independent tissue samples from litter-
979 matched male MacBlue and MacHDAC7 mice fed a chow diet.

FIGURE 1

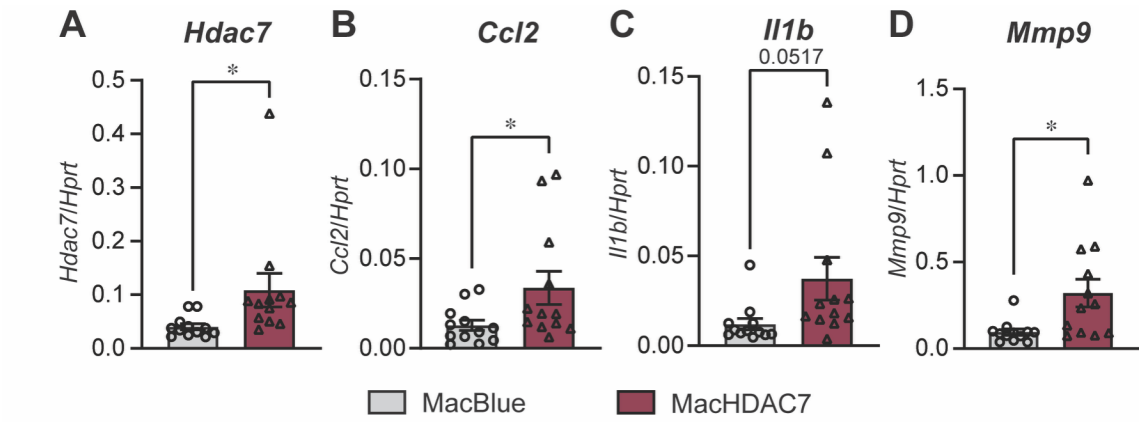
A
Hdac7
Hdac7/Hprt
0.5
0.4
0.3
0.2
0.1
0.0
*
B
Ccl2
Ccl2/Hprt
0.15
0.10
0.05
0.00
*
C
Il1b
0.0517
Il1b/Hprt
0.15
0.10
0.05
0.00
D
Mmp9
Mmp9/Hprt
1.5
1.0
0.5
0.0
*
MacBlue
MacHDAC7

FIGURE 2

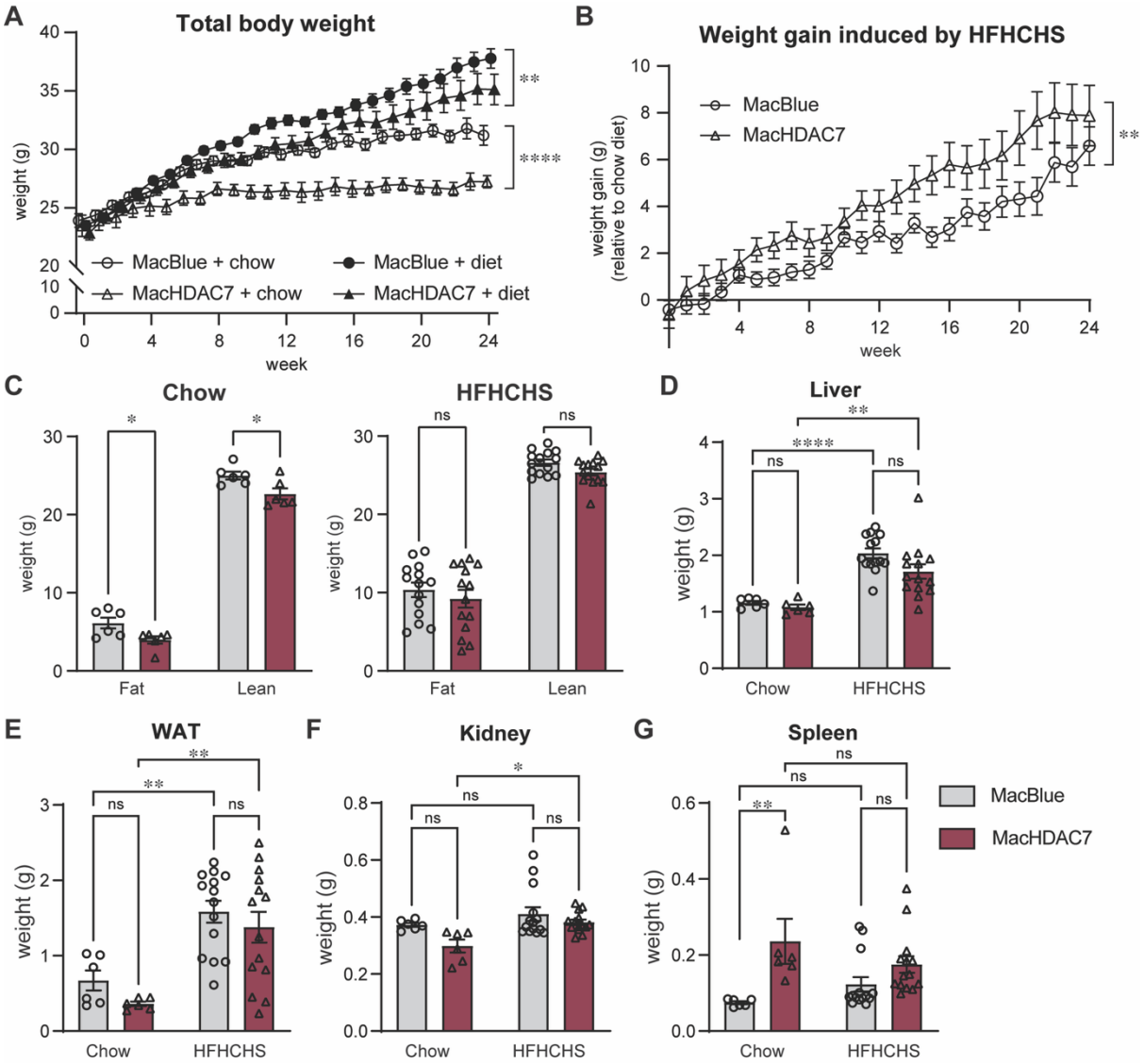
A
Total body weight
weight (g)
week
MacBlue + chow
MacHDAC7 + chow
MacBlue + diet
MacHDAC7 + diet
**
****
B
Weight gain induced by HFHCHS
weight gain (g)
(relative to chow diet)
week
MacBlue
MacHDAC7
**
C
Chow
HFHCHS
weight (g)
Fat
Lean
ns
D
Liver
Chow
HFHCHS
E
WAT
F
Kidney
G
Spleen
MacBlue
MacHDAC7

FIGURE 3

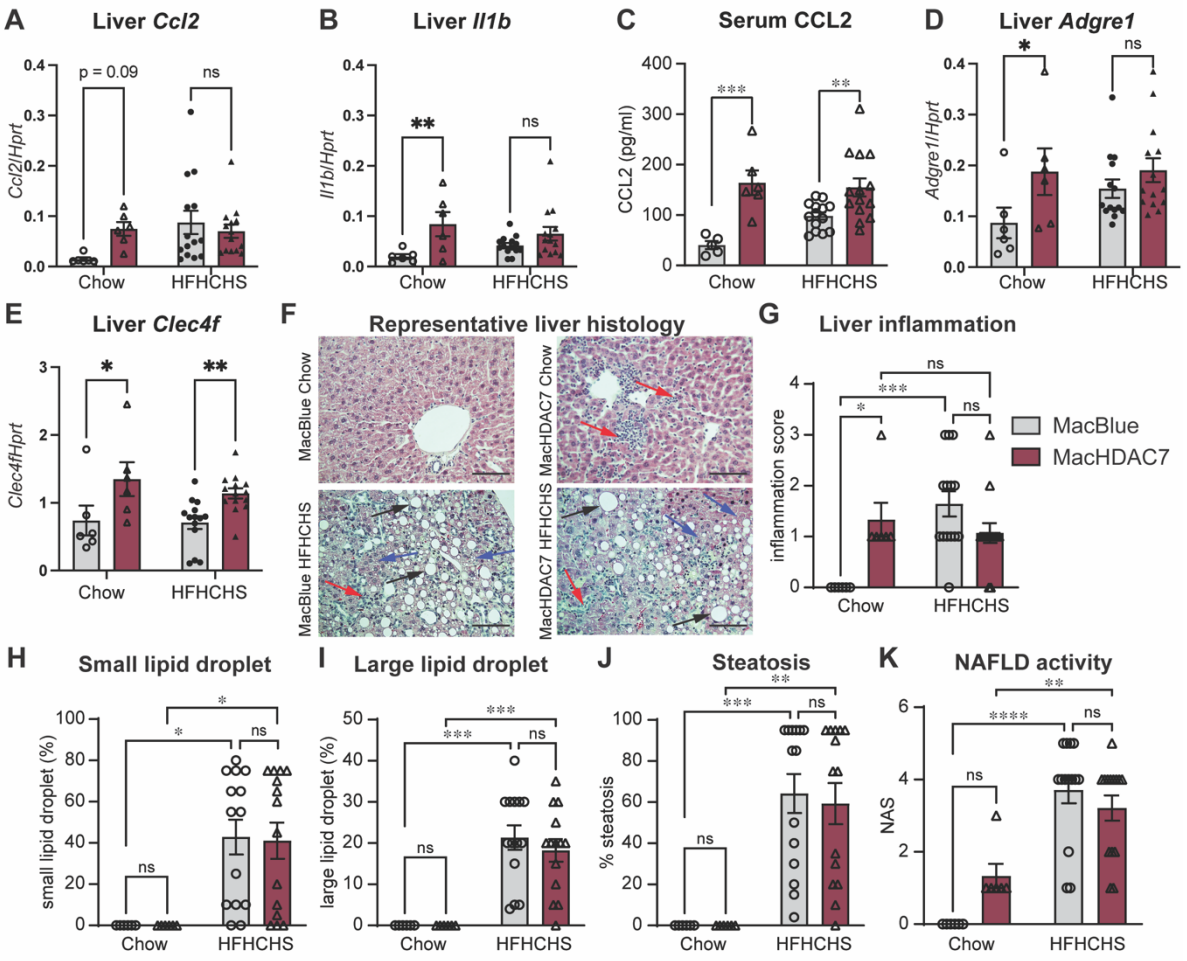
A
Liver Ccl2
Ccl2/Hprt
p = 0.09
ns
Chow
HFHCHS
B
Liver Il1b
Il1b/Hprt
**
ns
C
Serum CCL2
CCL2 (pg/ml)
***
**
D
Liver Adgre1
Adgre1/Hprt
*
ns
E
Liver Clec4f
Clec4f/Hprt
F
Representative liver histology
MacBlue Chow
MacHDAC7 Chow
MacBlue HFHCHS
MacHDAC7 HFHCHS
G
Liver inflammation
inflammation score
MacBlue
MacHDAC7
H
Small lipid droplet
small lipid droplet (%)
I
Large lipid droplet
large lipid droplet (%)
J
Steatosis
% steatosis
K
NAFLD activity
NAS

FIGURE 4

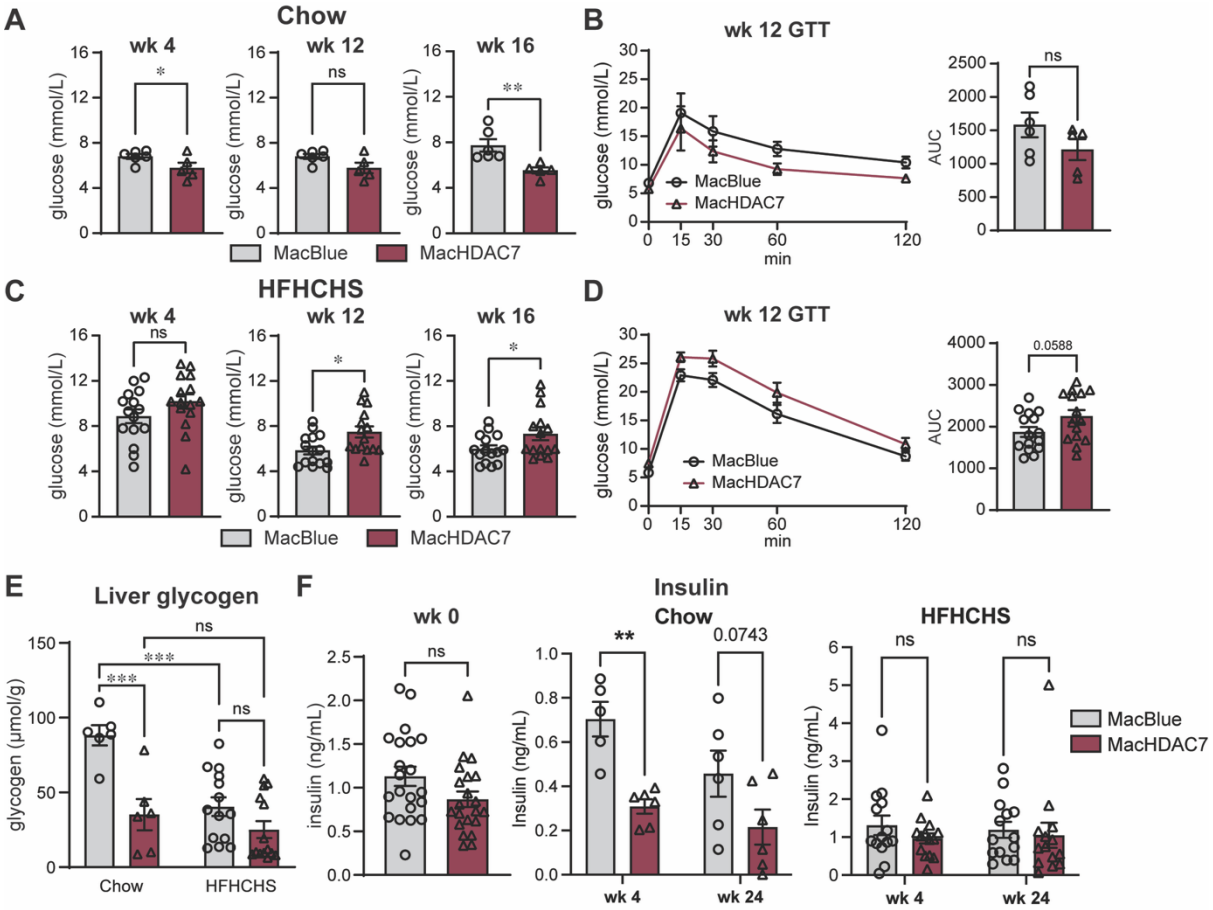
A
Chow
wk 4
wk 12
wk 16
glucose (mmol/L)
*
ns
**
MacBlue
MacHDAC7
B
wk 12 GTT
glucose (mmol/L)
MacBlue
MacHDAC7
min
AUC
ns
C
HFHCHS
wk 4
wk 12
wk 16
ns
*
*
D
wk 12 GTT
0.0588
E
Liver glycogen
glycogen (µmol/g)
***
***
ns
ns
Chow
HFHCHS
F
wk 0
Insulin
Chow
HFHCHS
insulin (ng/mL)
**
0.0743
wk 4
wk 24

FIGURE 5

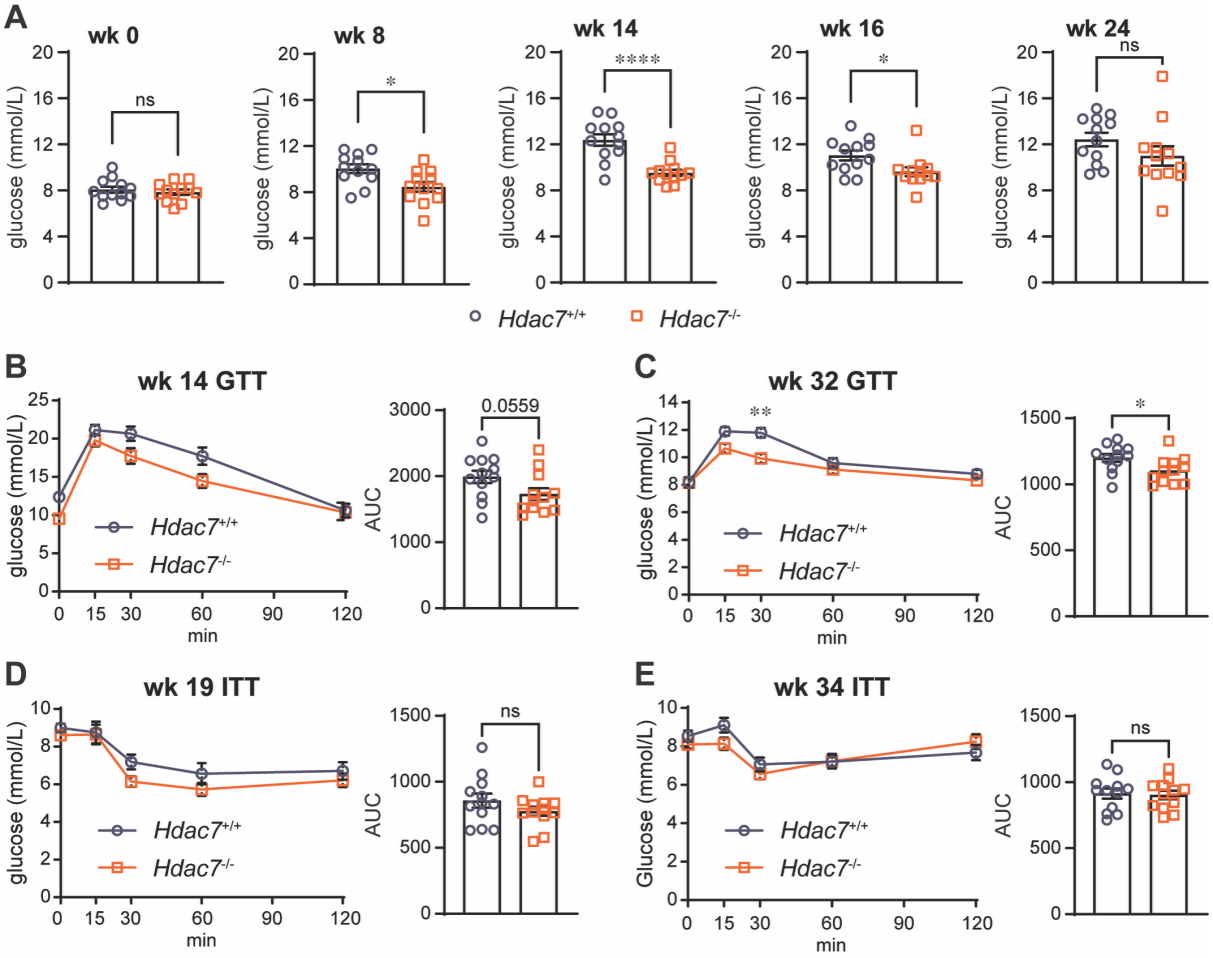
A
wk 0
wk 8
wk 14
wk 16
wk 24
glucose (mmol/L)
ns
*
****
*
ns
Hdac7+/+
Hdac7-/-
B
wk 14 GTT
glucose (mmol/L)
min
AUC
0.0559
C
wk 32 GTT
**
*
D
wk 19 ITT
ns
E
wk 34 ITT
Glucose (mmol/L)
ns

FIGURE 6

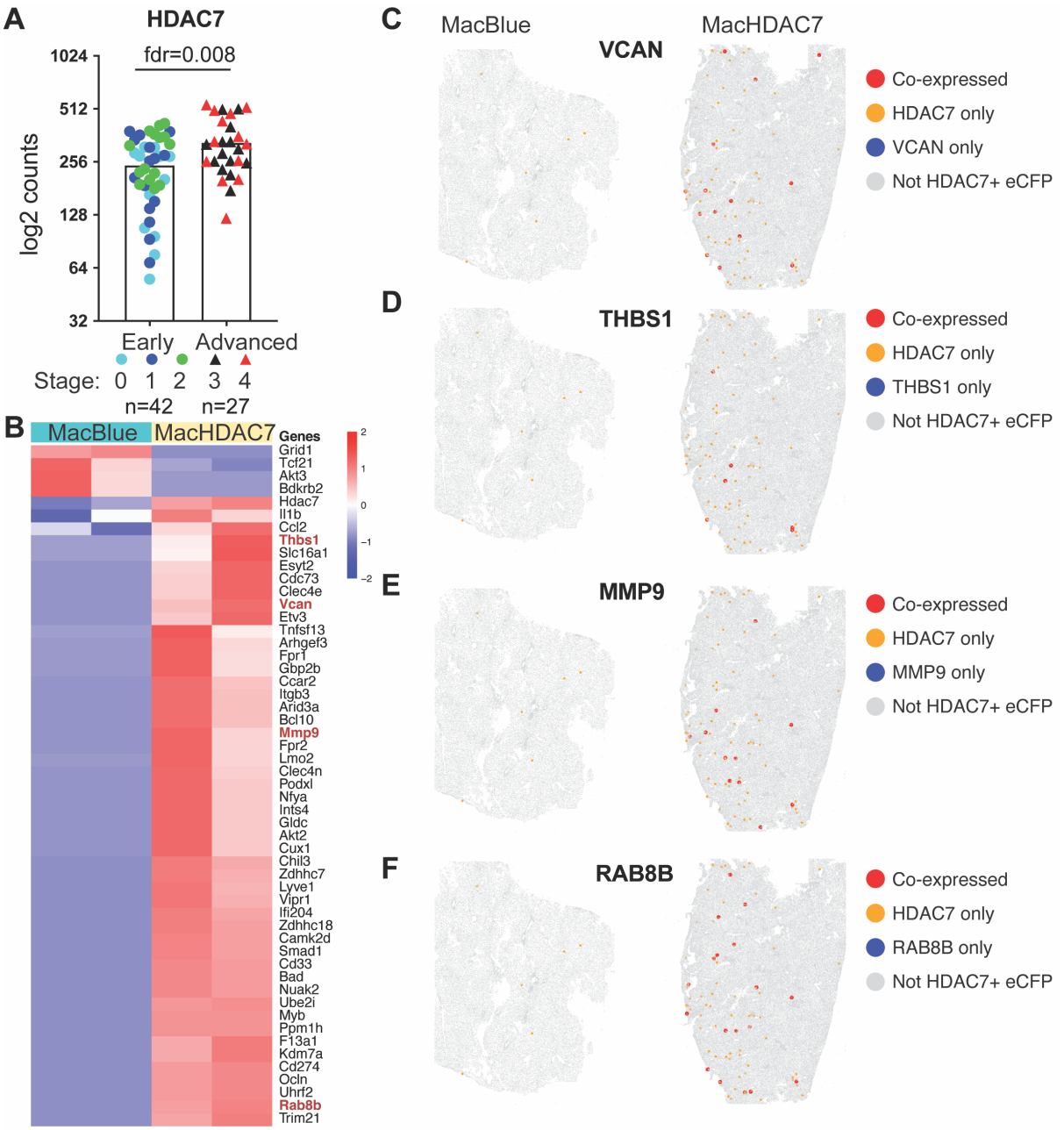
A
HDAC7
fdr=0.008
1024
512
256
128
64
32
log2 counts
Early
Advanced
Stage: 0 1 2 3 4
n=42
n=27
B
MacBlue
MacHDAC7
Genes
Grid1
Tcf21
Akt3
Bdkrb2
Hdac7
Il1b
Ccl2
Thbs1
Slc16a1
Esyt2
Cdc73
Clec4e
Vcan
Etv3
Tnfsf13
Arhgef3
Fpr1
Gbp2b
Ccar2
Itgb3
Arid3a
Bcl10
Mmp9
Fpr2
Lmo2
Clec4n
Podxl
Nfya
Ints4
Gldc
Akt2
Cux1
Chil3
Zdhhc7
Lyve1
Vipr1
Ifi204
Zdhhc18
Camk2d
Smad1
Cd33
Bad
Nuak2
Ube2i
Myb
Ppm1h
F13a1
Kdm7a
Cd274
Ocln
Uhrf2
Rab8b
Trim21
2
1
0
−1
−2
C
MacBlue
MacHDAC7
VCAN
Co-expressed
HDAC7 only
VCAN only
Not HDAC7+ eCFP
D
THBS1
Co-expressed
HDAC7 only
THBS1 only
Not HDAC7+ eCFP
E
MMP9
Co-expressed
HDAC7 only
MMP9 only
Not HDAC7+ eCFP
F
RAB8B
Co-expressed
HDAC7 only
RAB8B only
Not HDAC7+ eCFP

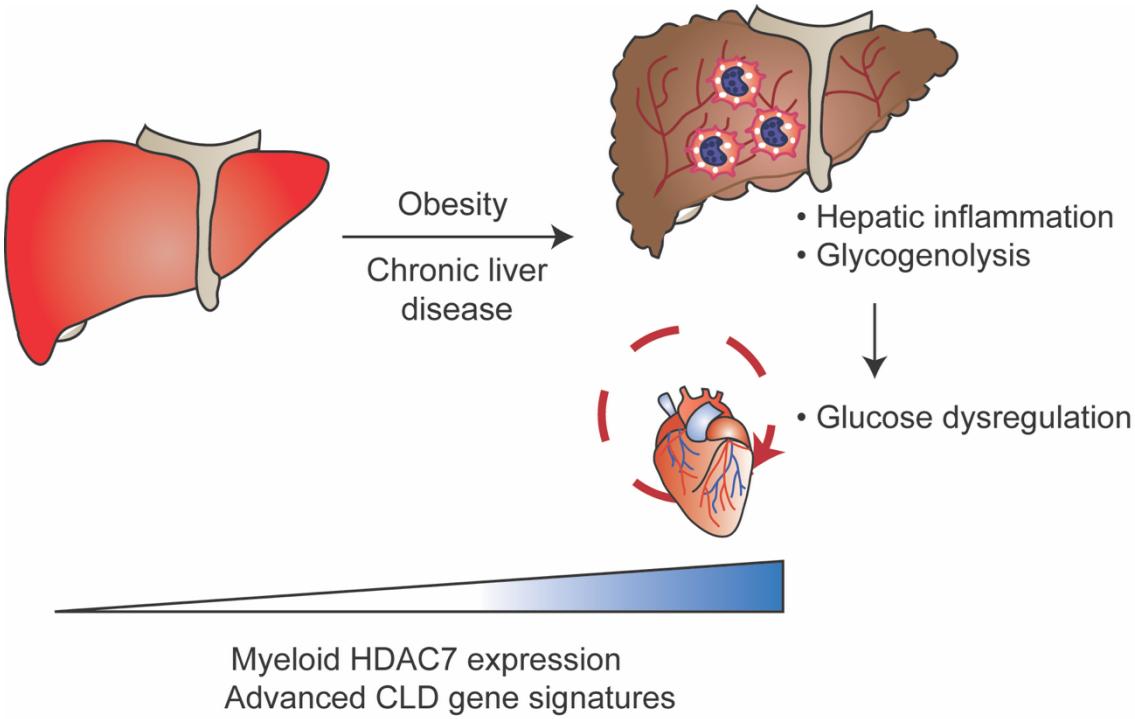

This study explored the role of the class IIa histone deacetylase HDAC7 in hepatic inflammation and metabolic disease. Genetic approaches in mice revealed that myeloid HDAC7 drives hepatic inflammation and gene signatures associated with advanced chronic liver disease. Myeloid HDAC7 also dysregulates systemic glucose metabolism during diet-induced obesity in mice.